

Europium, we have a problem

Modelling r-process enrichment across Local Group galaxies

M. Palla^{1,2,*}, M. Molero^{3,4}, D. Romano², and A. Mucciarelli^{1,2}

¹ Dipartimento di Fisica e Astronomia “Augusto Righi”, Alma Mater Studiorum, Università di Bologna, Via Gobetti 93/2, 40129 Bologna, Italy

² INAF, Osservatorio di Astrofisica e Scienza dello Spazio, Via Gobetti 93/3, 40129 Bologna, Italy

³ Institut für Kernphysik, Technische Universität Darmstadt, Schlossgartenstr. 2, Darmstadt 64289, Germany

⁴ INAF, Osservatorio Astronomico di Trieste, via Tiepolo 11, 34143 Trieste, Italy

Received 14 March 2025 / Accepted 28 May 2025

ABSTRACT

Context. Europium (Eu) serves as a crucial tracer in studying the origin of rapid neutron-capture process (r-process) elements. For this reason, extensive efforts have been made in the last decade to model the chemical evolution of this element in the Galaxy. However, far less attention has been reserved thus far for Eu in different galaxies of the Local Group.

Aims. By employing detailed and well-tested chemical evolution models, we investigate Eu enrichment across Local Group dwarf spheroidal galaxies, allowing for a direct comparison between model predictions for dwarf galaxies and the Milky Way.

Methods. Building upon an r-process enrichment framework that successfully reproduces the observed Eu abundance patterns, as well as the supernova and compact binary merger rates in the Milky Way, we built chemical evolution models for the Sagittarius, Fornax, and Sculptor dwarf spheroidal galaxies. We used these models to test the enrichment scenario against the abundance patterns observed in these galaxies.

Results. Models reproducing the Galactic Eu patterns significantly underestimate the [Eu/Fe] ratios observed in Local Group dwarfs. To address this ‘missing Eu’ problem, we estimated the Eu production rate needed to match the observations and explored the potential contributions either from prompt (core-collapse supernova like) or delayed (compact binary mergers) sources, assessing their compatibility with the Milky Way observables.

Conclusions. The same r-process enrichment frameworks cannot simultaneously reproduce the Eu patterns both in the Milky Way and in dwarf galaxies. However, a scenario where additional Eu is provided by an increased production from delayed sources at low metallicity can theoretically reconcile the trends observed in the Milky Way and in Local Group dwarfs. This is because of the small discrepancies (≤ 0.1 dex) between model predictions and observations found in this case. Further studies targeting and modelling of neutron-capture elements in Local Group galaxies are needed to fill the gaps in our current understanding of this problem.

Key words. nuclear reactions, nucleosynthesis, abundances – galaxies: abundances – galaxies: dwarf – galaxies: evolution – Local Group

1. Introduction

The majority of elements beyond the Fe peak are produced by neutron (n)-capture processes that can be rapid (r-process) or slow (s-process) with respect to the β -decay of the nuclei. Understanding the specific astrophysical sites of these two processes has become one of the major challenges in stellar physics and galactic chemical evolution. The main production sites of r-process elements, in particular, are still subject of intense study and debate (see Arcones & Thielemann 2023, for a review), with core-collapse supernova (CC-SN)-like objects, such as magnetorotationally driven SNe (hereafter, MRD-SNe, see e.g. Winteler et al. 2012; Nishimura et al. 2015, 2017; Reichert et al. 2021, 2023), collapsars (e.g. Siegel et al. 2019, and references therein), or magnetars (e.g. Patel et al. 2025), common-envelope jets SNe (CEJSNe, e.g. Grichener & Soker 2019; Grichener et al. 2022) as well as the merging of compact objects (neutron star-neutron star or neutron star-black hole; hereafter simply referred to as MNSs, e.g. Argast et al. 2004; Thielemann et al. 2017; Cowan et al. 2021) having been proposed.

Europium (Eu) is one of the few n-capture elements almost entirely built by the r-process (Burris et al. 2000; Bisterzo et al. 2011; Prantzos et al. 2020). The relatively easy detection of its absorption lines (compared to most of other n-capture elements, see discussion in e.g. Hansen et al. 2014, 2018; Lombardo et al. 2025; Alencastro Puls et al. 2025), together with the huge amount of time invested in Galactic observations (also through large spectroscopic surveys; e.g. Gaia-ESO, GALAH), has allowed us to extensively test the effect of these sources on the observed abundances. In this way, the concurrent production by CC-SN-like sources (also known as ‘prompt sources’) and MNSs (also known as ‘delayed sources’ due to their longer timescales; e.g. Côté et al. 2017; Hotokezaka et al. 2018; Simonetti et al. 2019; Greggio et al. 2021) has become a widely accepted scenario (e.g. Argast et al. 2004; Matteucci et al. 2014; Cescutti et al. 2015; Côté et al. 2019; Tsujimoto 2021; Molero et al. 2023; Van der Swaelmen et al. 2023).

The fairly solid theoretical explanation for the Eu abundance patterns in the Milky Way (MW) fostered the interest in this element as a potential chemical tag to discriminate between in situ and accreted populations in the stellar halo of the Galaxy (e.g.

* Corresponding author: marco.palla@inaf.it

Matsuno et al. 2021; Monty et al. 2024; Erandes et al. 2024), an interest reinforced also by the fact that it appears to be basically unaffected by the chemical processes internal to globular clusters (GCs, e.g. Roederer 2011; McKenzie et al. 2022).

Beyond the MW, ultra-faint dwarf (UFD) galaxies in the Local Group (LG), with typical metallicities $[\text{Fe}/\text{H}] \lesssim -2/-3$ dex (Ji et al. 2016a,b; Simon et al. 2023), provide excellent environments for unravelling the early galactic chemical evolution of the r-process elements, as due to the stochastic nature of the enrichment; namely, the limited number of nucleosynthetic events that enriched their oldest stars (e.g. Hartwig et al. 2019). Indeed, the very large scatter in abundances observed in these galaxies are among the few keys we can use in determining event occurrence rates and yield variations across different r-process sources (e.g. Alexander et al. 2023; Cavallo et al. 2023).

On the other hand, much less attention has been devoted to the theoretical study of n-capture elements at larger metallicities, namely, beyond the regime dominated by stochastic enrichment, in more massive satellites, namely, in the most massive dwarf spheroidal (dSph) galaxies. This is the case despite the good store of knowledge available on star formation and the general chemical evolution history of such objects (e.g. Lanfranchi & Matteucci 2004; de Boer et al. 2012, 2015; Vincenzo et al. 2014) and the number of observational programmes also targeting heavy elements (e.g. Letarte et al. 2010; McWilliam et al. 2013; Lemasle et al. 2014; Hill et al. 2019; Reichert et al. 2020 and references therein). Works on the theoretical interpretation of Eu abundances in dSph are in fact lacking, with only few studies focussed on the modelling of the evolution of heavy elements in these galaxies (e.g. Lanfranchi et al. 2008; Hirai et al. 2015; Vincenzo et al. 2015; Molero et al. 2021). The situation even worsens with respect to directly applying and comparing the modelling framework of r-process nucleosynthesis adopted for the MW to the chemical evolution of these galaxies. Skúladóttir & Salvadori (2020) studied the abundance patterns of Eu in Sagittarius, Fornax and Sculptor dSph in comparison to the ones in the Galaxy, proposing that the combination of quick+prompt and delayed r-process sources is able to self-consistently explain the chemical abundance pattern observed in the MW and its dwarf satellite galaxies. However, their adopted approach is purely schematic, without the implementation of any theoretical model. In fact, the same authors pointed out the need for follow-up studies including detailed chemical evolution modelling of both the MW and its dwarf satellite galaxies to investigate the r-process enrichment.

In this work, we focus on the theoretical interpretation of Eu enrichment in the three most massive dSph galaxies of the LG, namely, Sagittarius, Fornax, and Sculptor. We used detailed chemical evolution models that adopt the most recent and up-to-date prescriptions explaining the n-capture abundance patterns and measured CC-SN and MNS rates in the MW galaxy (Palla et al. 2020b; Molero et al. 2023). In this way, we can probe whether the accepted scenario to explain the Galactic constraints can be also applied to galaxies exhibiting different star formation histories (hereafter, SFHs) or modifications in the r-process enrichment framework are needed.

It is worth highlighting that this type of analysis is vital in the light of the use of Eu for chemical tagging (e.g. Matsuno et al. 2021; Monty et al. 2024). Other chemical elements routinely used for chemical tagging have well established production mechanisms, which can be tested on the abundance ratio patterns of different galaxies in diagrams such as the $[\alpha/\text{Fe}]$ versus $[\text{Fe}/\text{H}]$ (e.g. Matteucci & Brocato 1990; Matteucci 2012) or $[\text{Mg}/\text{Mn}]$ versus $[\text{Al}/\text{Fe}]$ (e.g. Horta et al. 2021; Fernandes et al. 2023,

but see also Vasini et al. 2024). Since a detailed knowledge of the element production sources would be required for a precise characterisation of the evolutionary path within a galaxy, it is crucial to extend the study of Eu to galactic ecosystems with different star formation and chemical evolution histories.

This paper is organised as follows. In Section 2, we present the data used to constrain the models. In Section 3, we discuss the model assumptions and ingredients, including the SFHs of different galactic systems and the nucleosynthesis prescriptions for n-capture elements. In Section 4, we describe in detail the r-process enrichment scheme that has been successfully tested against the data for the MW and apply it to the dwarf galaxies object of our study. Due to the systematic Eu underproduction that we find when implementing the Eu enrichment scheme for the MW in models for dwarf galaxies, in Sections 5 and 6, we quantify and explore the possible origin of the ‘missing Eu’ in these galaxies. Finally, in Section 7, we discuss our findings and present our main conclusions.

2. Observational data

In the following, we provide the details of the datasets adopted throughout this work to trace Eu enrichment in LG galaxies. Due to the different objects and extended metallicity intervals treated in this study, we lack homogeneous stellar sampling in terms of derivation of chemical abundances. Therefore, we chose to perform a careful collection of the best options available in the literature.

2.1. MW data

Despite the plethora of Galactic spectroscopic surveys in the last decade, we still lack a homogeneous sample of stars spanning the full metallicity range with measured Eu abundances, even for the Solar Neighbourhood. Therefore, in this work, we take advantage of abundance data from different surveys to sample the entire metallicity range within the Galaxy.

To sample the intermediate and metal-rich range ($[\text{Fe}/\text{H}] \geq -1.25$ dex), we considered chemical abundances from field stars and open clusters (OCs) in the Gaia-ESO survey (Gilmore et al. 2022; Randich et al. 2022). In particular, we selected field stars with Galactocentric radii in the range $7 < R_{\text{GC}}/\text{kpc} < 9$ (i.e. sampling the thick and thin disk in the solar region) with spectra obtained with UVES at high resolution, $\mathcal{R} \sim 47\,000$. Going into more detail, we considered stars from the sample of Viscasillas Vázquez et al. (2022), with the selection also described in Molero et al. (2023). For the OCs, instead, we adopted the sample of Gaia-ESO OCs from Magrini et al. (2023), comprising OCs older than 100 Myr (to avoid biases in abundance determination, see Spina et al. 2022; Magrini et al. 2023; Palla et al. 2024b), selected according to the Galactocentric radius cited above.

To sample the metal-poorer regime, we used stars from the Measuring at Intermediate metallicity Neutron-Capture Elements (MINCE) survey (Cescutti et al. 2022; François et al. 2024) and a collection of individual studies (Mishenina & Kovtyukh 2001; Hansen et al. 2012; Ishigaki et al. 2013; Roederer et al. 2014; Li et al. 2022), extracted from the Stellar Abundances for Galactic Archaeology (SAGA) database (‘SAGA’ stars, Suda et al. 2008). For the latter, we only considered studies targeting stars at a high spectral resolution ($\mathcal{R} \gtrsim 40\,000$), to select just the stars observed at comparable resolution to Gaia-ESO and MINCE (the latter with \mathcal{R} up to 100 000). In order to avoid contamination of stars from

accreted structures and consider only stars formed in situ in the metal-poor MW, we integrated the stellar orbits by adopting the McMillan (2017) potential and applied the same selection criteria for in situ stars as described in Monty et al. (2024). Finally, to avoid stars that are most likely polluted by an asymptotic giant branch (AGB) companion and, thus, do not reflect the chemical composition of their birth gas cloud, we selected only the stars with $[\text{Ba}/\text{Eu}] < 0$ and $[\text{Ba}/\text{La}] < 0$. Applying all the above mentioned selection criteria, we ended up with 1264 field stars and 13 OCs from the Gaia-ESO survey, 15 stars from MINCE and 39 ‘SAGA’ stars.

2.2. Dwarf galaxy data

As mentioned in Section 1, here we are considering the most massive and well observed dSphs in the LG, namely, Sagittarius, Fornax, and Sculptor. For all three galaxies, we selected abundances from studies based on high-resolution spectroscopy that provide Eu abundance determinations for a consistent number of stars (>30), spanning an extended metallicity range (>1 dex in $[\text{Fe}/\text{H}]$). For the full description of the samples, we refer to the original papers. However, we provide some details of the adopted datasets below:

- Sagittarius (Sgr): for this galaxy, we adopted the sample presented in Liberatori et al. (2025). The study presents 37 red-giant branch stars observed by means of the FLAMES-UVES high-resolution spectrograph ($\mathcal{R} \sim 47\,000$), all with available Eu abundances. The data cover a broad range of metallicities, namely, from $[\text{Fe}/\text{H}] \sim -2$ to ~ -0.4 dex, allowing us to sample all the main stellar populations of the galaxy. It is worth noting that the metal-poor stars in the sample were selected specifically to avoid contamination by the metal-poor globular cluster M54, which biases the abundance pattern of the Sgr dSph (see, e.g. Minelli et al. 2023 for a detailed discussion);
- Fornax (For): for this dSph, we took advantage of the sample presented in Reichert et al. (2020). The sample is built on a collection of spectra of red-giant branch stars, both from the archive and unpublished, obtained by means of the HIRES, UVES, and FLAMES-GIRAFFE spectrographs (all at a resolution of $\mathcal{R} \gtrsim 20\,000$). The spectra adopted in this study were processed in order to obtain homogeneous abundance measurements for all the targets (see Reichert et al. 2020 for the details). For For dSph, 128 stars are available, of which 108 had available Eu abundances, across the metallicity range of $-1.6 \leq [\text{Fe}/\text{H}]/\text{dex} \leq -0.4$;
- Sculptor (Scl): here, we used the study from Hill et al. (2019), with 99 red-giant branch stars in the center of the Scl dSph observed through FLAMES-GIRAFFE and FLAMES-UVES (all at resolution $\mathcal{R} \gtrsim 20\,000$) and with a homogeneous abundance analysis. Of these stars, 51 have available Eu abundances, across a metallicity distribution spanning $-2.1 \leq [\text{Fe}/\text{H}]/\text{dex} \leq -0.9$.

The trends in $[\text{Eu}/\text{Fe}]$ and $[\text{Eu}/\text{Mg}]$ versus $[\text{Fe}/\text{H}]$ for each of the galaxies considered in this work are shown in Fig. 1. The figure shows a different behaviour of the chemical pattern both depending on the galaxy and the abundance ratio we are looking at, namely $[\text{Eu}/\text{Fe}]$ (upper panel) and $[\text{Eu}/\text{Mg}]$ (lower panel). In particular, we clearly see that while Sgr and For show a similar trend in $[\text{Eu}/\text{Fe}]$ in comparison with the MW, the same is not seen for $[\text{Eu}/\text{Mg}]$, where the galaxies generally have higher abundances of $[\text{Eu}/\text{Mg}]$, with a stark overabundance, especially in Fornax at higher metallicities. On the other hand, Scl shows much lower $[\text{Eu}/\text{Fe}]$ ratios relative to those observed in the Galaxy at higher

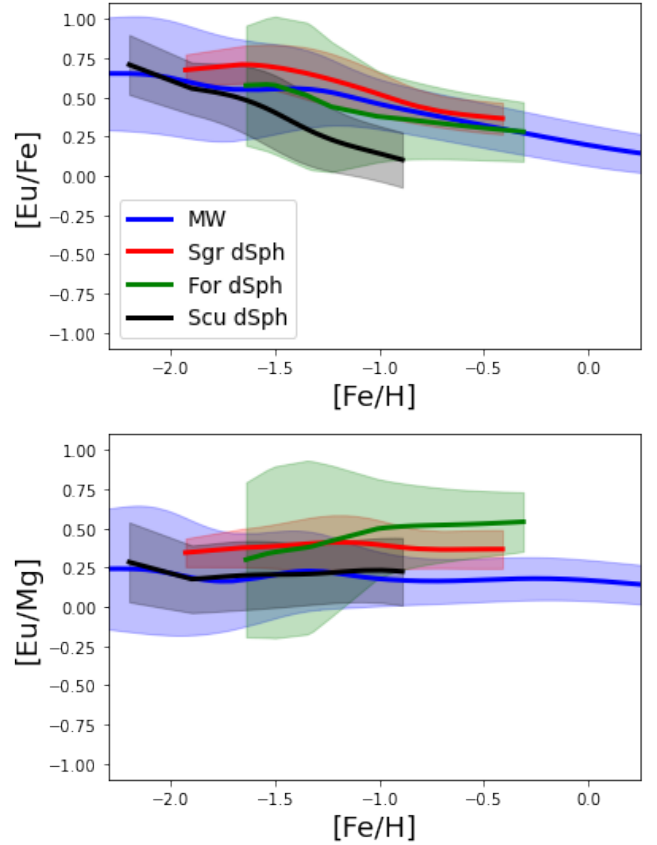


Fig. 1. $[\text{Eu}/\text{Fe}]$ (upper panel) and $[\text{Eu}/\text{Mg}]$ (lower panel) versus $[\text{Fe}/\text{H}]$ trends in the Local Group. The solid lines are non-parametric Gaussian KDE regressions computed for each galaxy basing on the datasets adopted throughout the paper. The shaded areas represent the 1σ confidence interval of the regressions.

metallicities. At the same time, $[\text{Eu}/\text{Mg}]$ is superposed to that of the Galaxy in the same metallicity interval. Despite the fact that in this work, we are focussed on the abundance ratios trends as function of $[\text{Fe}/\text{H}]$, it is worth noting that even considering $[\text{Mg}/\text{H}]$ on the x -axis, a similar relative behaviour in $[\text{Eu}/\text{Mg}]$ between different galaxies is also found. This, in turn, offers further confirmation of the characteristics observed in Fig. 1.

In this work we try to explain the above mentioned differences by using a detailed model of chemical evolution, considering the peculiar SFHs of the different galaxies and implementing different sources of Eu enrichment (prompt and delayed, see also Section 3). In particular, we tested whether the different SFHs alone can explain the differences in these trends, starting from models that exploit all the available constraints for r -process production (yields and event rates) and aptly reproduce the abundance patterns observed in our Galaxy.

It is worth mentioning that in Fig. 1 and throughout this work, all the abundances are rescaled to the solar ones by Grevesse & Sauval (1998). While this approach does not guarantee a fully uniform comparison (possible only with fully homogeneous datasets), this assures a first order of consistency, which is more than adequate for the purposes of this work.

3. Chemical evolution of r -process elements

In this section, we present the main prescriptions adopted to model the chemical evolution of r -process elements, especially

Eu, in different systems. In particular, in Section 3.1, we briefly summarize the main features of the chemical evolution models adopted for the solar vicinity and LG dwarf galaxies, whereas in Section 3.2 we focus on the prescriptions (e.g. stellar yields, delay-time-distributions) adopted for the enrichment sources of r-process elements.

3.1. Chemical evolution models

All the chemical evolution models discussed in this work rest on the following basic equation that describes the chemical evolution of a given element i (see e.g. [Matteucci 2012](#)):

$$\dot{G}_i(t) = -\psi(t)X_i(t) + R_i(t) + \dot{G}_{i,inf}(t) - \dot{G}_{i,out}, \quad (1)$$

where $G_i(t) = X_i(t)G(t)$ is the fraction of the gas mass in the form of an element, i , and $G(t)$ is the fractional gas mass; $X_i(t)$ represents the abundance fraction in mass of a given element, i , with the summation over all elements in the gas mixture being equal to unity.

The first term on the right-hand side of Eq. (1) corresponds to the rate at which an element, i , is removed from the ISM due to star formation. The star formation rate ($\psi(t)$, hereafter, SFR) is parametrised according to the Schmidt-Kennicutt law ([Kennicutt 1998](#)), with the star formation efficiency (SFE), represented by ν , as the control parameter that represents the SFR per unit mass of gas. Finally, $R_i(t)$ (see e.g. [Palla et al. 2020a](#) for the complete expression) takes into account the nucleosynthesis from different stellar sources, weighted according to the initial mass function (IMF). This term also includes the products originating from binary systems such as MNSs (see Section 3.2) and Type Ia SNe. For the latter, we assume the delay-time-distribution (DTD) by [Matteucci & Recchi \(2001\)](#), which enables us to obtain abundance patterns that are similar to those obtained with other literature Type Ia SNe DTDs (see e.g. [Matteucci et al. 2009](#); [Palla 2021](#) for details).

The last two terms of Eq. (1) refer to the gas flows history of the galaxy, namely, the inflows and outflows, for which different prescriptions are adopted depending on the specific history of star formation of the galaxies under scrutiny (see Sections 3.1.1 and 3.1.2). In general, we modelled the rate of gas inflow in terms of an exponentially-decaying law (see e.g. [Romano et al. 2010](#); [Palla et al. 2020a](#); [Kobayashi et al. 2020](#)) as

$$\dot{G}_{i,inf} = C_{inf} X_{i,inf} e^{-t/\tau_{inf}}, \quad (2)$$

where C_{inf} is the normalization constant, which is set to reproduce the total gas mass accreted by the infall, $X_{i,inf}$ is the chemical abundance of the element, i , of the infalling gas; here, it assumed to be primordial and τ_{inf} is the infall timescale. With respect to the galactic winds, we assume them to be proportional to the SFR (e.g. [Vincenzo et al. 2015](#); [Molero et al. 2021](#); [Palla et al. 2024a](#)) as

$$\dot{G}_{i,out} = \omega_i \psi(t), \quad (3)$$

where ω_i is the mass-loading factor-free parameter, assumed to be the same for all chemical elements i . For the MW, $\omega_i = 0$ (see [Melioli et al. 2009](#); [Spitoni et al. 2009](#); [Hopkins et al. 2023](#)).

All the galaxy models adopted in this work adopt the same IMF and nucleosynthesis prescriptions. For the IMF, we use the one from [Kroupa et al. \(1993\)](#). The galaxy-wide IMF (gwIMF) of dwarf galaxies might be different from that derived from local star counts (see e.g. [Jeřábková et al. 2018](#), and references

therein). Hence, we explored alternative IMF formulations, however, they did not help to solve the Eu problem. Therefore, we do not discuss the issue of gwIMF variations further. Concerning the stellar yields, we adopt those by [Karakas \(2010\)](#) for low- and intermediate-mass stars, [Nomoto et al. \(2013\)](#) for massive stars, and [Iwamoto et al. \(1999\)](#) for Type Ia SNe. For the sources of production of n-capture elements, we refer to Section 3.2.

3.1.1. MW galaxy

To model the evolution of the solar vicinity, we adopted the best model of [Palla et al. \(2020b\)](#), which was already implemented to study the evolution of n-capture elements in the MW disk by [Molero et al. \(2023\)](#). The model is a revised version of the two-infall paradigm ([Chiappini et al. 1997, 2001](#), see also [Spitoni et al. 2019](#)), in which two consecutive gas accretion episodes, separated by an age gap of 3.25 Gyr, form the so-called high- α and low- α sequences observed in the Galactic disk.

In this scenario, the first infall takes place on a relatively short timescale ($\tau_{inf} = 1$ Gyr) and high SFE, ($\nu = 2$ Gyr $^{-1}$), while the second gas-infall episode happens on longer timescales ($\tau_{inf} \simeq 7$ Gyr) and lower SFE ($\nu = 1.3$ Gyr $^{-1}$) in accordance with what claimed by several studies for the solar vicinity (e.g. [Spitoni et al. 2020](#); [Palla et al. 2022](#); [Romano et al. 2021](#), see also e.g. [Marcon-Uchida et al. 2010](#); [Kobayashi et al. 2020](#) for similar consideration on the Galactic thin disk modelling). Indeed, these assumptions allowed to reproduce large survey abundance data ([Palla et al. 2020b](#); [Spitoni et al. 2021](#)), as well as abundance-age diagrams ([Spitoni et al. 2019, 2020](#)) in the Solar Neighbourhood, also with a good agreement with present-day rates of star formation and SNe (see e.g. [Molero et al. 2023](#) and references therein).

The reproduction of the typical $[\alpha/\text{Fe}]$ abundance pattern in the solar vicinity can be observed in Fig. 2, where we compare the predictions of the two-infall model in the $[\text{Mg}/\text{Fe}]$ versus $[\text{Fe}/\text{H}]$ diagram with abundances from the data samples described in Section 2.1. In the figure, we clearly see the typical loop (or ribbon) feature being due to the delayed gas accretion episode forging the low- α sequence (see e.g. [Spitoni et al. 2019](#)), well in agreement with the bulk of MW disk stars and OCs (the latter tracing stars younger than ~ 5 Gyr) in the solar region. The comparison with low-metallicity, in-situ stars also assure us that we neither significantly underestimate or overestimate the level of the $[\alpha/\text{Fe}]$ plateau, therefore preventing any initial substantial bias when we are looking to elements, which are much more uncertain in terms of their nucleosynthetic origin.

3.1.2. Local group dSphs

To model the chemical evolution of LG dSph, we followed previous chemical evolution works by [Molero et al. \(2021\)](#) for Fornax and Sculptor and [Mucciarelli et al. \(2017\)](#); [Minelli et al. \(2023\)](#) for Sagittarius. Below, we summarize the main model assumptions for the three galaxies:

- Sagittarius (Sgr): we assume a rather long lasting, single episode of star formation for this galaxy, from ~ 14 to 6 Gyr ago, after which the Sgr galaxy stops forming new stars, in agreement with results by [Dolphin \(2002\)](#) and [de Boer et al. \(2015](#), but see also [Siegel et al. 2007](#)). We assume an infall timescale of $\tau_{inf} = 3$ Gyr and a SFE of $\nu = 0.2$ Gyr $^{-1}$ from ~ 14 to 7 Gyr ago, after which the star-formation rate drops abruptly ($\nu = 0.001$ Gyr $^{-1}$). This is largely due to gas stripping (for which we assume a mass loading factor of $\omega = 2$) caused by the interaction with the Galaxy (see

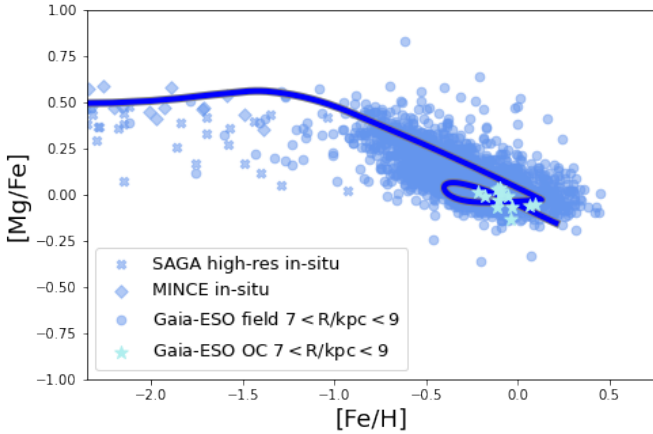


Fig. 2. [Mg/Fe] versus [Fe/H] for the MW. Data are from high-resolution SAGA data selection (see Section 2.1, light blue crosses), MINCE (Cescutti et al. 2022, light blue diamonds), Gaia-ESO field stars (light blue points, Viscasillas Vázquez et al. 2022), and Gaia-ESO open clusters (cyan stars, Magrini et al. 2023).

Minelli et al. 2023, for details), starting 7.5 Gyr ago in the model. The tidal stripping also impacts the dSph stellar populations, forming the Sgr stream we observe at the present-day (e.g. Monaco et al. 2007; de Boer et al. 2015). Because the adopted dataset for Sgr samples the Sgr main body (see Minelli et al. 2023), we remove 50% of the stars with [Fe/H] < -0.6 dex in accordance with Law & Majewski (2016, and references therein, see also Minelli et al. 2023), who showed that tidal stripping removes preferentially metal-poor stars from the Sgr main body;

- Fornax (For): for this galaxy we take into consideration the SFH derived by de Boer et al. (2012) from colour-magnitude diagram (CMD) fitting analysis, according to which Fornax formed stars at all ages, from as old as 14 Gyr to as young as 0.25 Gyr. For this reason, we model a continuous star formation, characterized by one single long episode lasting 14 Gyr, with infall timescale and SFE equal to $\tau_{inf} = 2.25$ Gyr and $\nu = 0.125$ Gyr⁻¹, respectively, also assuming galactic winds with mass loading factor of $\omega = 1$ (Molero et al. 2021). With such a SFH, the model predicts a present-day stellar mass of $M_* = 3.1 \cdot 10^7 M_\odot$, very similar to the one estimated by de Boer et al. (2012), $M_* = 4.3 \cdot 10^7 M_\odot$;
- Sculptor (Scl): as for the SFH of Scl, we rest on the CMD fitting analysis by Bettinelli et al. (2019). These authors show that most of Scl stars are formed in a single episode of star formation ending ~9–10 Gyr ago. We model this SFH with an initial burst ($\nu = 0.1$ Gyr⁻¹) driven by rapid infall of gas ($\tau_{inf} = 0.5$ Gyr) and a subsequent decline driven by galactic winds, with a mass-loading factor of $\omega = 2.5$. In this way, the predicted final stellar mass is $M_* = 2.6 \cdot 10^6 M_\odot$, in agreement with the observed one, $M_* = 2.24 \cdot 10^6 M_\odot$ (Bettinelli et al. 2019, see also de Boer et al. 2012).

The above theoretical prescriptions allow us to reproduce the observations available for the different systems. This is shown in Fig. 3, where we compare observed and predicted [Mg/Fe] versus [Fe/H] abundance patterns and metallicity distribution functions (MDFs) for Sgr (top panels), For (central panels) and Scl (bottom panels) dSphs. The observed MDFs are from Minelli et al. (2023) for Sgr and Molero et al. (2021) for For and Scl; more details can be found in the original papers.

In general, we observe that the set of parameters adopted for the three systems reproduce well the data trends in the [Mg/Fe]

vs [Fe/H] diagrams (Fig. 3 left panels), also considering the observational uncertainties and the non-uniform sampling in metallicity (especially for For). The agreement between observed and modelled abundance patterns demonstrates the suitability of our adopted single-episode SFHs to explain the evolution of these dSphs, without advocating to more complex SFH (an therefore, abundance patterns), as for the two-infall scenario for the MW. A remarkable agreement is also obtained between the predicted MDFs and the measured ones (Fig. 3 right panels). This is further confirmed by looking at the predicted and observed median distributions: the two are almost overlapping in all the three panels, showing a maximum deviation of ≈ 0.15 dex for Scl.

Despite the large uncertainties in the SFH measurements of the three LG galaxies (e.g. Siegel et al. 2007; de Boer et al. 2012, 2015) and the theoretical limitations of our pure chemical models in tracking the complex chemo-dynamical evolution of the galaxies, it is important to stress that the simultaneous reproduction of both $[\alpha/\text{Fe}]$ versus [Fe/H] abundance patterns and MDFs allows us to place stringent constraints on the evolutionary paths of these systems (see e.g. the discussion in Romano et al. 2015). Therefore, the above mentioned limitation are not expected to strongly affect our conclusions regarding the evolution of n-capture elements in these galaxies. Indeed, the understanding of the nucleosynthetic origin of the elements beyond the Fe-peak is very limited, making the uncertainties on elemental nucleosynthesis much more relevant than the ones arising from the SFHs of the galaxies.

3.2. r-process elements nucleosynthesis

As explained in Section 3.1, all the models adopt the same nucleosynthesis prescriptions for n-capture elements. As Eu is the main topic of this work and it is a typical r-process element (produced at ~97% by the r-process at solar system formation, Burris et al. 2000), we focus on r-process nucleosynthesis only in this work.

We consider two channels for the production of r-process elements: MNSs and MRD-SNe. In particular, MNSs are computed as systems of two neutron stars of $1.4 M_\odot$ with progenitors in the 9–50 M_\odot mass range. Their rate is computed as the convolution between a given DTD and the SFR (see Molero et al. 2021, 2023):

$$R_{MNS}(t) = k_\alpha \int_{\tau_i}^{\min(t, \tau_s)} \alpha_{MNS} \psi(t - \tau) f_{MNS}(\tau) d\tau, \quad (4)$$

where k_α is the number of neutron-star progenitors per unit mass in a stellar generation (0.0041 for a Kroupa et al. 1993 IMF), α_{MNS} is the fraction of stars in the correct mass range which can give rise to a double neutron-star merging event, set to $2 \cdot 10^{-3}$ as reference (Molero et al. 2023), and f_{MNS} is the DTD of MNSs. For the DTD, we adopt the formulation of Simonetti et al. (2019, see also Greggio et al. 2021), where the nuclear lifetime of the secondary progenitor component accounts for an initial plateau lasting up to 40 Myr. This is followed by a power-law decay proportional to t^{-1} , a form commonly used in chemical evolution studies (e.g. Côté et al. 2019; Cavallo et al. 2021), which accounts for systems where the delay is primarily driven by gravitational radiation.

The yields of r-process elements from MNSs have been obtained by scaling to solar the yield of Sr measured in the re-analysis of the spectra of the kilonova AT2017gfo by Watson et al. (2019, after having considered uncertainties in its derivation; see Molero et al. 2021 for details). The Eu yield

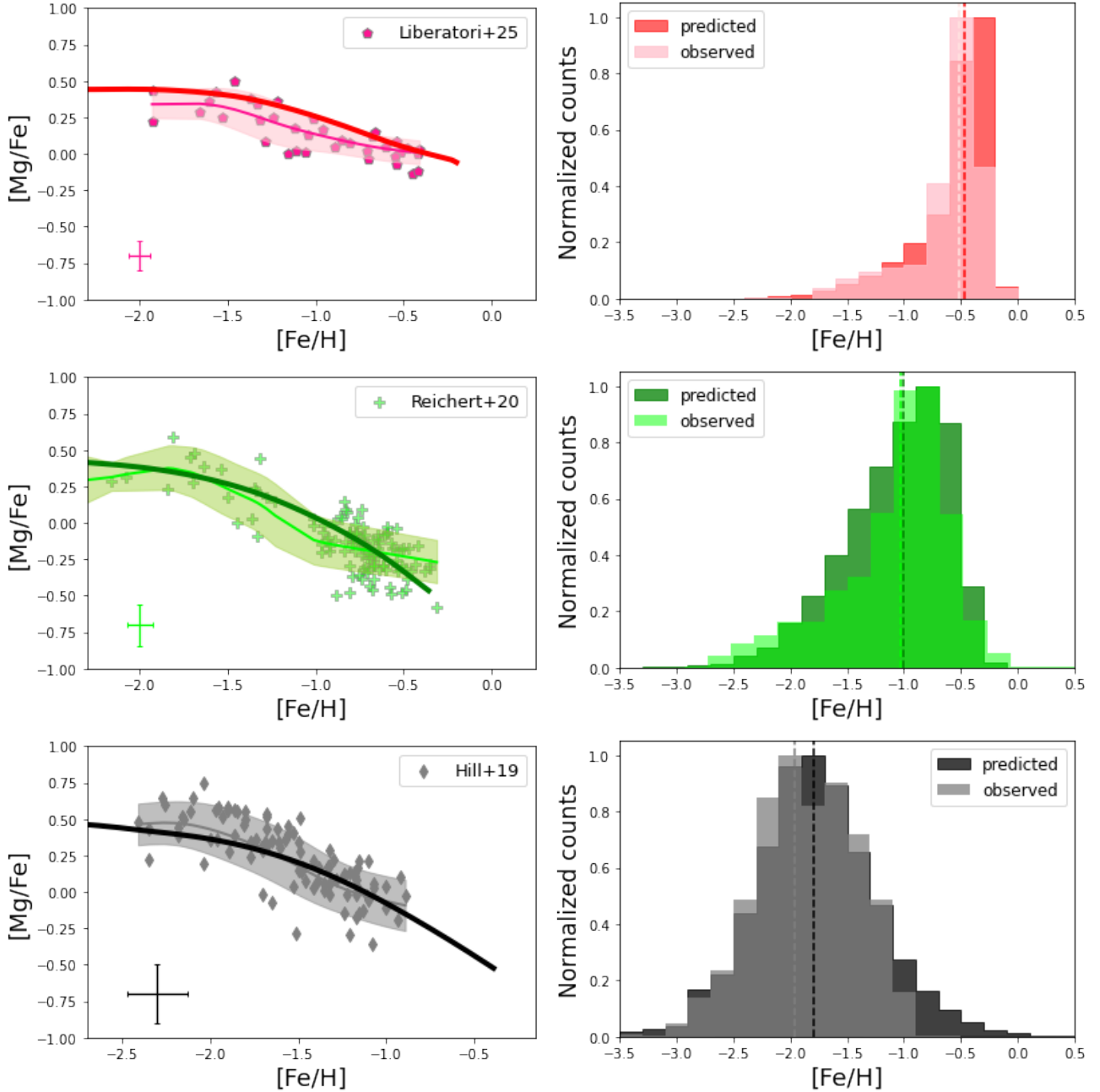


Fig. 3. $[\text{Mg}/\text{Fe}]$ vs. $[\text{Fe}/\text{H}]$ (left panels) and MDF (right panels) for Sagittarius (top panels) Fornax (central panels) and Sculptor (bottom panels). Data for $[\text{Mg}/\text{Fe}]$ vs. $[\text{Fe}/\text{H}]$ are from Liberatori et al. (2025) for Sagittarius, Reichert et al. (2020) for Fornax and Hill et al. (2019) for Sculptor. The thin solid lines and shaded areas represent the non-parametric Gaussian KDE data regressions and their 1σ confidence interval for $[\text{Mg}/\text{Fe}]$ vs $[\text{Fe}/\text{H}]$. The thick solid lines are the model predictions. For sake of comparison with observations, in this and the following figures we show theoretical $[\text{X}/\text{Fe}]$ vs $[\text{Fe}/\text{H}]$ curves for the first 99% of the predicted cumulative distribution of stars. Observed MDFs are from Minelli et al. (2023) for Sagittarius and Molero et al. (2021) for Fornax and Sculptor.

obtained in this way is $Y_{\text{Eu}}(\text{MNS}) = 3 \cdot 10^{-6} M_{\odot}$ (per merging event), also consistent with the theoretical calculation of Korobkin et al. (2012) and with estimates from Matteucci et al. (2014).

For what concerns MRD-SNe, here we assume that they originate from a fraction of stars in the mass interval between 10 and 80 M_{\odot} . This fraction is regulated by the α_{MRD} parameter, which is set to 0.2 as in Molero et al. (2023), fine-tuned to reproduce the r-process pattern in the MW disk. The set of yields adopted for the MRD-SNe is the model L0.75 of

Nishimura et al. (2017), also chosen to be consistent with the best-fitting model of Molero et al. (2023) for the MW disk.

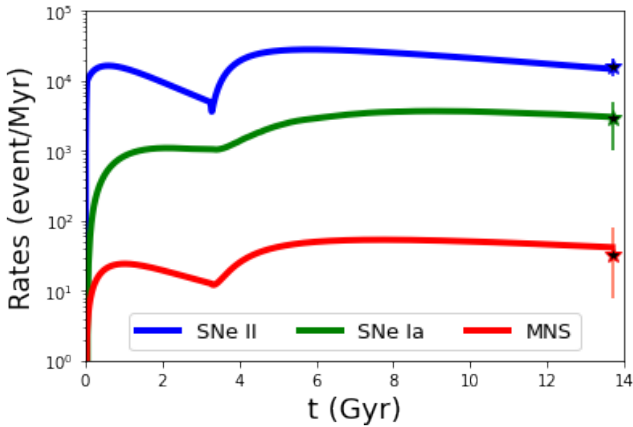
4. A well-behaved model for the MW

In this section, we show the predicted behaviour of Eu enrichment for the galaxies object of our study under the scenario that best reproduces the $[\text{Eu}/\text{Fe}]$ versus $[\text{Fe}/\text{H}]$ average trend in the solar vicinity. The parameters concerning the r-process nucleosynthesis, namely the fraction of progenitors (for MNSs and

Table 1. Main parameters for r-process enrichment in the calibrated MW disk model (Molero et al. 2023).

α_{MNS}	$Y_{Eu}(MNS)^{(1)}$	α_{MRD}	$Y_{Eu}(MRD)^{(2)}$
$2 \cdot 10^{-3}$	$3 \cdot 10^{-6} M_{\odot}$	0.2	$4.69 \cdot 10^{-7} M_{\odot}$

Notes. ⁽¹⁾ Molero et al. (2021), ⁽²⁾ Nishimura et al. (2017).

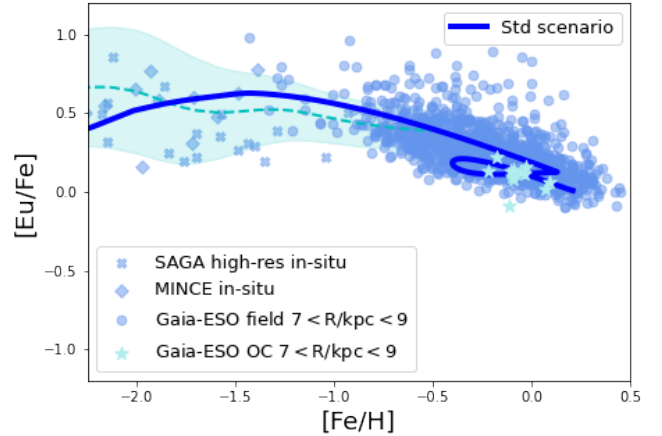

Fig. 4. Predicted evolution of CC-SN, Type Ia SN and MNS rates in the MW compared with present-day observations from Rozwadowska et al. (2021, CC-SNe), Cappellaro et al. (1997, Type Ia SNe) and estimate from Abbott et al. (2021, MNSs), respectively.

MRD-SNe) in the right mass interval and the yields, are listed in Table 1.

4.1. Reproducing the Galactic constraints

Having fixed the DTD function (see Section 3.2) and the SFR behaviour for the MW (from the two-infall model, see Section 3.1.1), the adopted fraction of systems originating a MNS (α_{MNS}) allows us to well reproduce the measured rate of MNS in the Galaxy. This is shown in Fig. 4, where we report the predictions of the MW model for the rates of CC-SN, Type Ia SN and MNS compared to the observations (all averaged over the whole disc). It is worth noting that for MNSs, we consider the cosmic rate observed by Abbott et al. (2021), namely, $320_{-240}^{+490} \text{ Gpc}^{-3} \text{ yr}^{-1}$, converting it to a Galactic rate (see Section 5.2 in Simonetti et al. 2019 for details on the derivation). The obtained rate for the MW ($32_{-24}^{+49} \text{ Myr}^{-1}$) is also in agreement within the error bars with the rate of Kalogera et al. (2004) from binary pulsars.

In Fig. 5, we show instead the predictions for the [Eu/Fe] versus [Fe/H] trend in the solar vicinity, as compared to the data for the MW described in Section 2. It is worth noting that in this figure (as well as the following ones), we limit the metallicity to values greater than [Fe/H] = -2.5 dex. This is because we are not interested in the scatter caused by the stochastic enrichment of Eu that characterizes the very metal-poor regime (e.g. Cescutti et al. 2015; Wanajo et al. 2021, see also Section 1). Rather, the goal of this work is to study and reproduce the trend of stars at metallicities [Fe/H] ≥ -2 dex, namely, at metallicities where the chemical mixing starts to be effective (e.g. Schönrich & Weinberg 2019) and the scatter is more likely to be dominated by measurement errors (see e.g. Molero et al. 2023).


Fig. 5. [Eu/Fe] vs [Fe/H] for the solar vicinity. Data are a selection from the SAGA database (light blue crosses; see Section 2.1), MINCE (light blue diamonds, François et al. 2024), Gaia-ESO field stars (light blue points, Viscasillas Vázquez et al. 2022), and Gaia-ESO open clusters (cyan stars, Magrini et al. 2023). The cyan thin dashed line and shaded area represent the non-parametric Gaussian KDE data regressions and its 1σ confidence interval. The thick solid blue line are the predictions of the standard model for the MW (see text).

Referring back to Fig. 5, we stress that the r-process enrichment scenario adopted here is in good agreement with the data trend over the entire metallicity range of interest, from low metallicities ([Fe/H] ~ -2 dex) up to the metallicities observed in Galactic disk field stars and OCs. In particular, the latter trace the enrichment in the Galactic disk in the last few Gyrs and they are very well reproduced by the typical loop (ribbon) feature caused by the delayed second infall episode (see also Fig. 2 and Spitoni et al. 2019; Palla et al. 2020b; Molero et al. 2023).

The simultaneous reproduction of Galactic rates and chemical abundance patterns confirm the results of previous studies who claimed that both prompt and delayed Eu sources are needed to reproduce the observations (e.g. Matteucci et al. 2014; Cescutti et al. 2015; Côté et al. 2019; Tsujimoto 2021; Molero et al. 2023; Van der Swaelmen et al. 2023). However, it is worth noting that the prompt source for Eu enrichment, here represented by MRD-SNe (alternative sources are collapsars, e.g. Siegel et al. 2019 and references therein), dominates over the enrichment by MNSs (see also Van der Swaelmen et al. 2023). Indeed, by computing the present mass fraction of Eu in the ISM produced by individual sources, we get $X(\text{Eu})_{MNS} = 5.6 \cdot 10^{-11}$ and $X(\text{Eu})_{MRD} = 5.2 \cdot 10^{-10}$, namely only $\approx 10\%$ of the total Eu budget is produced by delayed sources such as a MNS. In turn, this indicates a limited impact of MNSs in shaping the observed [Eu/Fe] abundance patterns in the MW (see also Molero et al. 2023).

4.2. Applying the scenario to LG dSphs

Next, we applied the prescriptions for r-process enrichment that explain the Galactic rates and Eu abundance patterns to the dwarf galaxies that are the subject of this study. Such an approach was already adopted to the modelling of r-process in dwarfs (e.g. Vincenzo et al. 2015; Molero et al. 2021), and stems from the fact that, at variance with the MW, no MNS rate estimation can be inferred directly / derived in a straightforward manner (Kalogera et al. 2004; Simonetti et al. 2019) for these systems.

The obtained [Eu/Fe] versus [Fe/H] abundance patterns for Sgr, For and Scl dSphs are shown in Fig. 6 (top, central, and

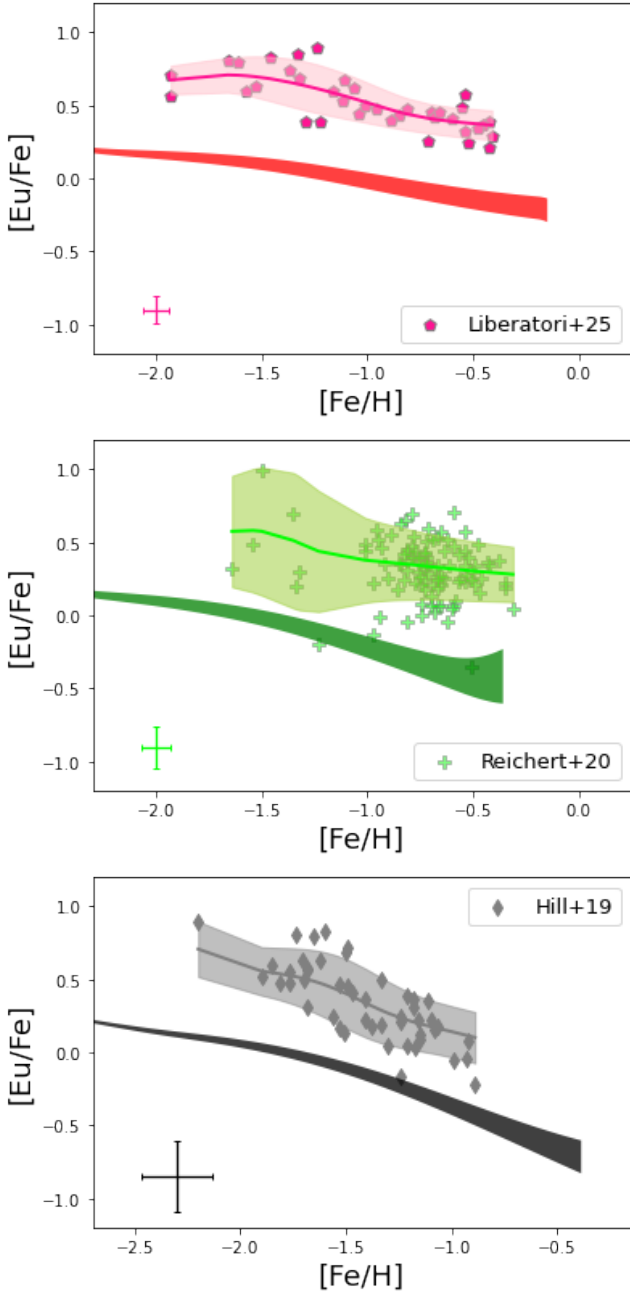


Fig. 6. [Eu/Fe] vs [Fe/H] for Sagittarius (top panel), Fornax (central panel), and Sculptor (bottom panel). Data for are from [Liberatori et al. \(2025\)](#) for Sagittarius, [Reichert et al. \(2020\)](#) for Fornax, and [Hill et al. \(2019\)](#) for Sculptor. The dark shaded areas are the range of predicted values, adopting the reference MNS yield and a MNS yield that is a factor of 5 greater to account for the uncertainties in MNS yield measurements by [Watson et al. \(2019\)](#). The thin solid lines and light shaded areas represent the non-parametric Gaussian KDE data regressions and their 1σ confidence interval for [Eu/Fe] vs [Fe/H].

bottom panels, respectively). In all the panels, we show the range of predicted values adopting the reference MNS yield (see Table 1) and a factor of 5 greater MNS yield; namely, within the uncertainties in MNS yield measurements by [Watson et al. \(2019\)](#), and also described by [Molero et al. \(2021\)](#). It is evident that the three models show a marked deficiency in Eu production with respect to what is observed, with a typical underestimation of [Eu/Fe] relative to the data regression by ~ 0.5 dex in all

systems. Even a factor of 5 increase in the MNS yield does not help in reducing significantly the large displacement between the observed and predicted [Eu/Fe] trends.

Therefore, the r-process enrichment scenario that best reproduces the measurements in the solar vicinity has severe limitations when dealing with other galactic systems. It is worth stressing that such inconsistency between Galactic and extra-Galactic trends has not been pointed out before (see e.g. [Skúladóttir & Salvadori 2020](#); [Molero et al. 2021](#); [Ernandes et al. 2024](#)). Earlier works studying the MW galaxy were basing on previous MNS rate measurements ([Kalogera et al. 2004](#); [Abbott et al. 2017](#), see e.g. [Simonetti et al. 2019](#); [Grisoni et al. 2020](#)). Indeed, the present-day MNS rate by [Abbott et al. \(2017\)](#) provides order of magnitude larger values relative to more up to date measurements ($R_{MNS} = 154^{+320}_{-122} \text{ Myr}^{-1}$ instead of $R_{MNS} = 32^{+49}_{-24} \text{ Myr}^{-1}$). This means that larger α_{MNS} (of the order of $\gtrsim 10^{-2}$) have to be adopted in the models for the MW to fit the present-day Galactic MNS rate. Therefore, previous studies on dwarf galaxies that apply α_{MNS} as inferred to reproduce the earlier MNS rate in the MW (e.g. [Molero et al. 2021](#)) achieve a satisfactory agreement with the observed abundances. However, as stated above, a reassessment of the observed MNS rate necessitates reducing the probability of MNS events (i.e. reducing α_{MNS}) in the model, ultimately making MNSs an inefficient channel for r-process production.

In turn, an increase in the MNSs contribution to Eu enrichment by increasing the α_{MNS} parameter should alleviate the tension between models, as changes to delayed sources contribution potentially have stronger effects in the abundance ratios of dwarf galaxies than more massive ones, due to the time-delay model (see [Matteucci 2012, 2021](#)). Indeed, the slower rate of metal enrichment would allow for more Eu accumulation by delayed sources at low-metallicities, boosting the [Eu/Fe] to larger values. However, just increasing the α_{MNS} parameter across the whole time evolution is not a viable solution, as it would cause an overestimation of the present-day MNS rate in the Galaxy measured by [Abbott et al. \(2021\)](#).

5. The missing Eu in LG dSphs

The model for the dwarfs of the LG show a clear lack of Eu, as illustrated in Fig. 6. In this section, we try to estimate the missing rate of Eu production of our model within the three dwarf galaxies analysed in this work.

Without making any hypothesis on the origin of this lack of r-process element production, we run a grid of models where we add a fictitious source producing Eu up to a [Fe/H] threshold (hereafter, $[\text{Fe}/\text{H}]_{\text{thresh}}$):

$$\text{'Missing Eu' rate} = \begin{cases} x & \text{if } [\text{Fe}/\text{H}] \leq [\text{Fe}/\text{H}]_{\text{thresh}} \\ 0 & \text{if } [\text{Fe}/\text{H}] > [\text{Fe}/\text{H}]_{\text{thresh}} \end{cases}, \quad (5)$$

where x is the ‘missing Eu’ production rate normalised to the SFR. For the gridding scheme, we adopted an array with respective spacing of 0.05 dex for $[\text{Fe}/\text{H}]_{\text{thresh}}$ and $5 \cdot 10^{-11}$ for the ‘missing Eu’ x . We modelled this additional production rate per unit SFR, in order to compare directly the values we find in the different galaxies we model. For the grid of models, we computed their likelihood relative to the observed Eu abundance trends for each individual galaxy (Sgr, For and Scl), as well as the total weighted likelihood for the three galaxies together (see Appendix A for the details of the calculation).

The approach described above may appear simplistic, as the missing production rate of r-process may vary depending on

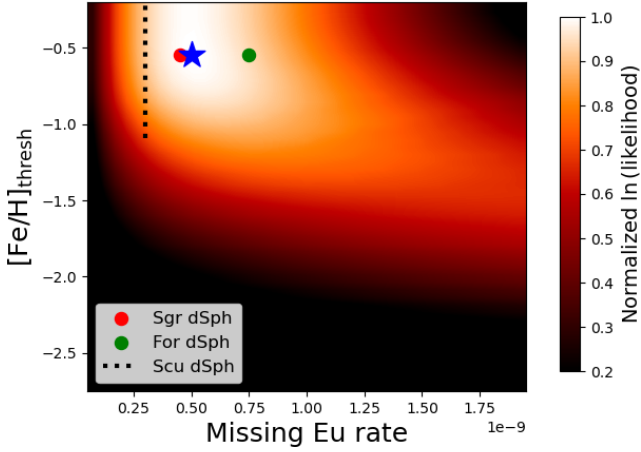


Fig. 7. Total weighted likelihood for the sample dwarf galaxies as function of the ‘missing Eu’ rate (normalised to the SFR) and metallicity threshold $[\text{Fe}/\text{H}]_{\text{thresh}}$. The model setup with maximum total weighted likelihood is indicated with the blue star. Setups with maximum likelihood for Sagittarius, Fornax and Sculptor are indicated with a red point, a green point and a dashed line, respectively.

metallicity (or time) with a more complex shape than the heavy-side step function adopted in Eq. (5) as seen in previous studies (see e.g. Fig. 2 of Côté et al. 2019). However, some arguments can be put forward to justify our choice, for instance: (i) the data samples adopted for the different dSph are limited in size (≤ 100 stars per galaxy): this is at variance with typical samples for the MW, which can count on thousands of stellar sources, allowing more sophisticated statistical analysis. ii) Eu abundances are measured for stars in a restricted metallicity range (i.e. it is not possible to probe Eu evolution across the whole metallicity range as inferred from the galaxy’s MDF). It is difficult to properly sample the missing Eu budget in different metallicity intervals and it is also worth noting that the main goal of this analysis is to give a first estimate of this missing Eu budget. In fact, this is the first time that the problem is illustrated from the theoretical point of view. Therefore, it is important to give a first estimate, before proceeding with a more in-depth analysis.

The results of the likelihood computation are shown in Fig. 7. In particular, we show the colormap for the total weighted likelihood, together with the models obtaining the maximum likelihood for the individual galaxies. The ‘missing Eu’ rate needed to reconcile the observed $[\text{Eu}/\text{Fe}]$ trends with the model predictions is similar for the different dwarf galaxies (within a factor of ~ 2 difference, see symbols in Fig. 7). The best models for individual galaxies are also in line with the maximum total weighted likelihood for the sample, giving a ‘missing Eu’ rate (normalised to the SFR) of $5 \cdot 10^{-10}$. The analysis also highlights that this additional Eu production must be in place up to a metallicity of $[\text{Fe}/\text{H}] = -0.55$ dex. We notice that the Scl stellar distribution extends only up to $[\text{Fe}/\text{H}] \sim -1$ dex (see Fig. 3) and this is why the likelihood on the metallicity threshold axis for this galaxy is not reliable above this metallicity. This is why we find that Scl models with $[\text{Fe}/\text{H}]_{\text{thresh}} \geq -1.05$ dex have the same likelihood for a given ‘missing Eu’ rate.

In summary, we can say that in LG dwarfs up to metallicities $[\text{Fe}/\text{H}] \sim -0.5$ dex an additional Eu production rate (normalised to the SFR) of $5 \cdot 10^{-10}$ is needed. However, we need to consider what this value means in comparison to the rate of Eu production by other sources. In Fig. 8, we show the rate of Eu production (normalized to the galaxies SFRs) by MNSs and MRD-SNe as

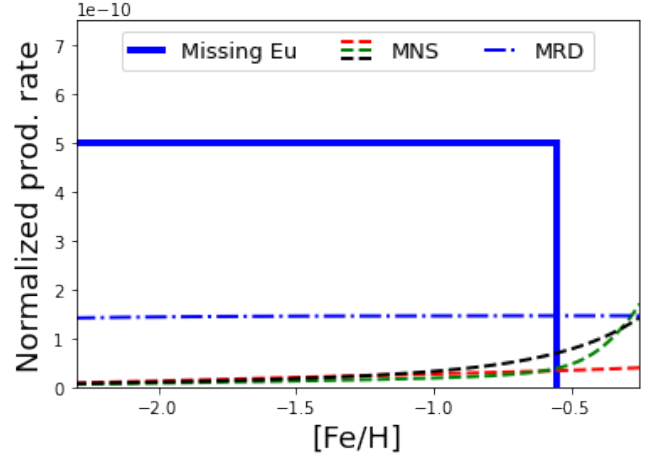


Fig. 8. Eu production rate normalised to the SFR by different sources (missing Eu: thick solid line, MNSs: dashed lines, MRD-SNe: dash-dotted line) in the models for LG dSphs with maximum total weighted likelihood (blue star in Fig. 7). Different Eu production rates by MNSs are found for different galaxies (black: Scl, green: For, red: Sgr) due to their different SFHs (see text).

compared to the ‘missing Eu’ that explains the observed trends in LG dSphs.

As it stands, it is clear that to explain the high $[\text{Eu}/\text{Fe}]$ values observed in these galaxies we need to boost the Eu production rate by a factor of ≈ 4 relative to the combined contribution of MRD-SNe and MNSs that we use to explain the data in the MW. In fact, MNSs start to significantly pollute the ISM only at late times (and, therefore, large metallicities) due to their typical delay-times (see Section 3.2), with a contribution dependent on the different SFH shape in different galaxies (see the different line colours in Fig. 8). On the contrary, prompt MRD-SNe naturally track the SFR (which implies no differences in the normalized production rates among galaxies), but they are not sufficient to explain the $[\text{Eu}/\text{Fe}]$ ratios observed in the three dwarf galaxies.

6. The origin of the missing Eu

In this section, we investigate in more detail the ‘missing Eu’ problem. In particular, we suggest a novel Eu enrichment scenario that explains the abundance ratios observed in LG dwarfs in light of the two classes of candidates for Eu production, namely, delayed sources (MNSs) and prompt ones (here represented by MRD-SNe). After devising such an alternative scenario, we tested it against the abundance trends observed in the MW. In this way, we can probe whether or not we can attribute the different patterns observed in different galaxies not only to their different SFH (as due to the time-delay model), but also to intrinsic differences in the properties of their stellar populations (e.g. fraction of binary systems leading to MNSs).

6.1. A potentially larger MNS contribution at low metallicity

To reproduce the high abundance of Eu observed in LG dSphs, here we test the hypothesis of an increased contribution to Eu production by MNSs at low metallicities, possibly due to an increased rate of formation of MNS progenitor systems (however, an increased yield per MNS event can also contribute to the Eu boost). The hypothesis of an increase in the number of MNS progenitors has already been made in other works

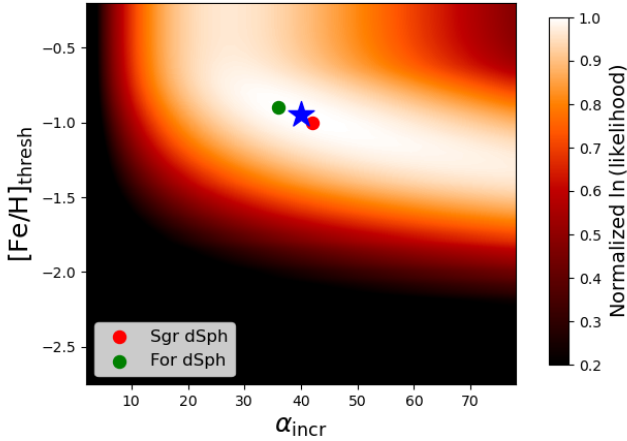


Fig. 9. Total weighted likelihood for the sample dwarf galaxies as function of the increase factor in the α_{MNS} parameter α_{incr} and metallicity threshold $[\text{Fe}/\text{H}]_{\text{thresh}}$. Symbols in legend are the same as in Fig. 7.

about the chemical evolution of Eu and r-process in general (e.g. Simonetti et al. 2019; Cavallo et al. 2021) and stems from results of binary population synthesis models (e.g. Bogomazov et al. 2007; Mennekens & Vanbeveren 2014), showing that metallicity plays a crucial role in the formation of compact-object binaries (Giacobbo & Mapelli 2018). However, previous assumptions on the dependence of the MNS rate on metallicity did not rely on a quantitative analysis of the available data samples.

Here, we try to fill this gap by running a grid of models for Sgr and For (for Scl, its limited metallicity distribution does not allow to perform a meaningful likelihood analysis; see more details later in this section) increasing the fraction of systems in the right mass interval giving rise to MNS events, i.e. α_{MNS} , up to a given metallicity threshold, $[\text{Fe}/\text{H}]_{\text{thresh}}$. In particular, we varied the α_{MNS} parameter introduced in Eq. (4) in this way:

$$\alpha_{MNS} = \begin{cases} 2 \cdot 10^{-3} \times \alpha_{incr} & \text{if } [\text{Fe}/\text{H}] \leq [\text{Fe}/\text{H}]_{\text{thresh}} \\ 2 \cdot 10^{-3} & \text{if } [\text{Fe}/\text{H}] > [\text{Fe}/\text{H}]_{\text{thresh}} \end{cases}, \quad (6)$$

where α_{incr} is a multiplicative factor applied to the $\alpha_{MNS} = 2 \cdot 10^{-3}$ parameter introduced in Table 1. Concerning the gridding scheme, we adopted an array with spacing of 0.05 dex for $[\text{Fe}/\text{H}]_{\text{thresh}}$ and 2 for α_{incr} , respectively. It is worth noting that the step function in metallicity adopted in Eq. (6) may be seen as a simplistic approximation, as a more gradual decreasing trend is expected for the fraction of these systems (see e.g. Giacobbo & Mapelli 2018). However, we stuck to the above approximation as our goal is to give a first-order quantitative estimate for the decrease of the α_{MNS} parameter. Considering more elaborated functional forms is beyond the scope of this paper, as it would require a larger set of higher quality data.

We proceeded as done in Section 5 and computed the likelihood for the grid of models relative to the observed abundance trends (see Appendix A). The results of the likelihood computation are shown in Fig. 9. It can be appreciated that for both For and Sgr dSph the α_{MNS} parameter has to be multiplied by a large multiplication factor ($\alpha_{incr} > 30$) up to a metallicity of $[\text{Fe}/\text{H}] \approx -1$ dex. Here, the lower metallicity threshold (it was $[\text{Fe}/\text{H}]_{\text{thresh}} \approx -0.5$ dex in the case of the ‘missing Eu’ rate estimation; see previous section) can be explained in the light of the delayed nature of MNSs. In fact, MNS progenitor systems forming at $[\text{Fe}/\text{H}] < [\text{Fe}/\text{H}]_{\text{thresh}}$ can pollute the ISM at much larger metallicities than the adopted threshold. Concerning the individual galaxies, For shows an increase in MNSs

extended up to larger $[\text{Fe}/\text{H}]$ relative to Sgr (-0.9 dex and -1 dex, respectively), but with relatively lower α_{incr} values (36 and 42, respectively). The lower α_{incr} seems in contradiction with the larger ‘missing Eu’ rate found for For relative to Sgr ($7 \cdot 10^{-10}$ and $4.5 \cdot 10^{-10}$ respectively, see Fig. 7). However, such a difference can be explained by the larger contribution to Eu production by MNSs in For relative to Sgr for metallicities above $[\text{Fe}/\text{H}] > -1$ dex (see Fig. 8): in fact, the weight of an increased MNS rate on the Eu production will be larger in For relative to Sgr, therefore allowing slightly lower α_{incr} values. In any case, it is worth reminding that the (small) difference we found can be also partly due to the limited size of the data samples and/or uneven metallicity sampling (see e.g. Fig. 6, central panel). Therefore, we can conclude that the best values found for the two galaxies are compatible with each other.

The $[\text{Eu}/\text{Fe}]$ and $[\text{Eu}/\text{Mg}]$ versus $[\text{Fe}/\text{H}]$ patterns obtained by the best models (both total weighted, solid lines, and for individual galaxies, dashed lines) as found by the maximum likelihood analysis are shown in Fig. 10. These are compared with the ‘standard’ scenario discussed in Section 4 (dotted lines). The large increase in the fraction of systems giving rise to MNS events allows to reconcile the model predictions for both For and Sgr with the observed trends, which are instead severely underestimated in the case of the ‘standard’ scenario. Reassuringly, we note that the observed trends are well recovered both by the best models for the individual galaxies and by the model with parameters from the maximum total weighted likelihood. This suggests that, rather than focusing on such details as the exact value of the α_{incr} parameter, we first ought to fix our attention on the key result of our analysis, namely, the need for a very large boost in Eu production by MNSs at low metallicities.

At variance with the approach adopted in Sect. 5, we do not perform the same analysis done for Sgr and For for Scl dSph, as the limited metallicity distribution of Scl (ending at $[\text{Fe}/\text{H}] \sim -1$ dex) does not allow to obtain a meaningful result from the likelihood computation (see Fig. 7). Nonetheless, it is fundamental to apply the best model derived for Sgr and For to Scl, to check the consistency of the proposed enrichment scenario for Eu in LG dwarfs.

The $[\text{Eu}/\text{Fe}]$ and $[\text{Eu}/\text{Mg}]$ versus $[\text{Fe}/\text{H}]$ patterns obtained for Scl dSph with the Eu enrichment setup as found by the maximum likelihood analysis on Sgr and For is shown in Fig. 11. Also in the case of Scl, the new scenario (solid lines) agrees within the 1σ confidence interval of the observed trends for $[\text{Fe}/\text{H}] \gtrsim -2$ dex. In contrast, in the ‘standard’ scenario (dotted lines), the general trend is severely underestimated for both $[\text{Eu}/\text{Fe}]$ and $[\text{Eu}/\text{Mg}]$. It is also worth reminding that here we focus on the trends for $[\text{Fe}/\text{H}] \gtrsim -2$ dex (see Section 3), as at lower metallicities stochastic effects heavily affect the observed abundance patterns (e.g. Cescutti et al. 2015; Schönrich & Weinberg 2019). Moreover, in Scl the $[\text{Fe}/\text{H}] \lesssim -2$ dex range is probed only by a single star (Hill et al. 2019, see also Appendix B for other datasets) and therefore slight discrepancies in this metal regime should not worry us much.

6.2. Exploring prompt sources at low metallicity

The other possibility we consider to explain the abundance trends in LG dwarf galaxies is a larger contribution from prompt sources, here represented by MRD-SNe (e.g. Winteler et al. 2012; Nishimura et al. 2015, 2017). Nonetheless, in this section, we also checked possible yields and rates from collapsars, as they represent a common framework for prompt r-process sources in

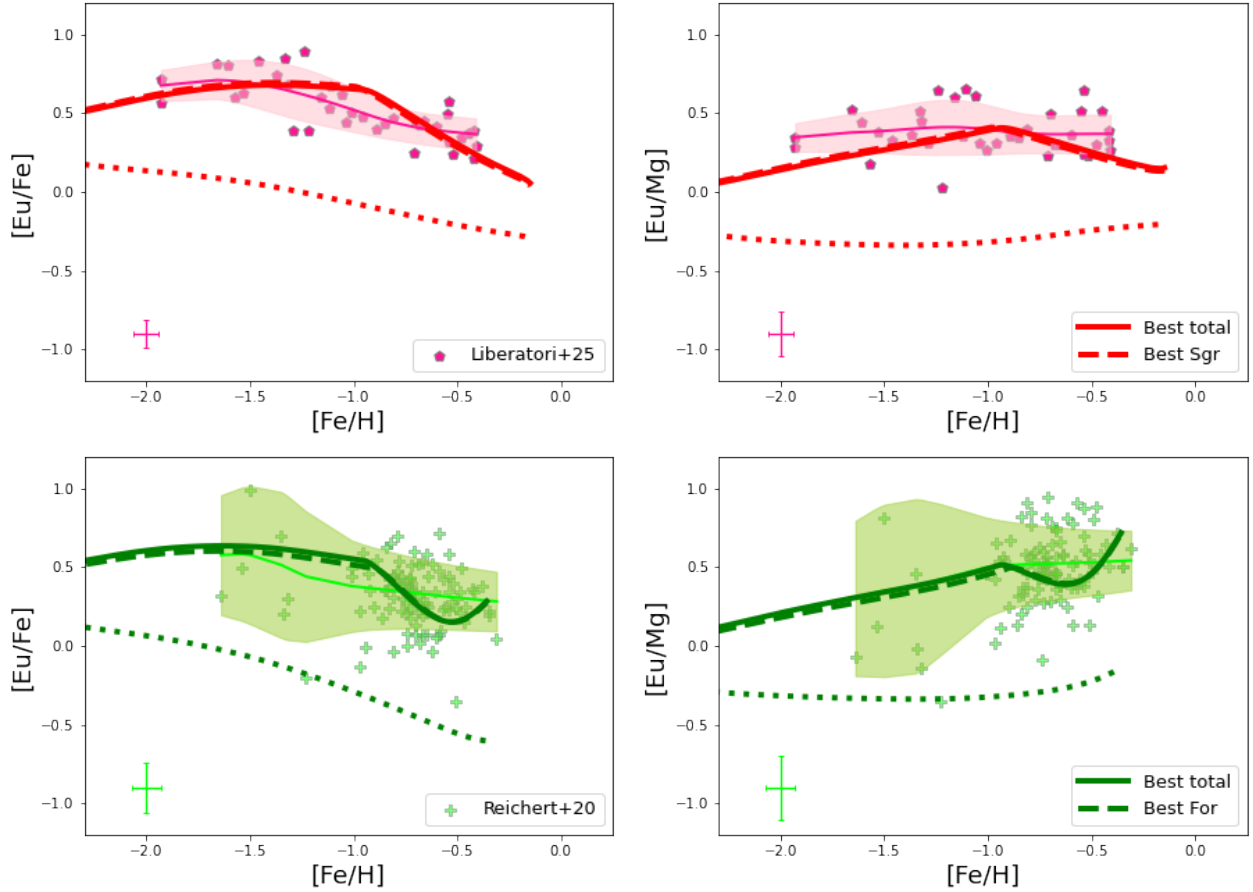


Fig. 10. [Eu/Fe] versus [Fe/H] (left panels) and [Eu/Mg] versus [Fe/H] (right panels) for Sagittarius (top panels) and Fornax (bottom panels) for models with increased MNS production at low metallicity. Solid lines represent evolutionary tracks for models with Eu enrichment setup with maximum total weighted likelihood, while dashed lines models with maximum likelihood for the individual galaxy. For comparison, the models with standard Eu enrichment setup are also shown (dotted lines). The legend is the same as in Fig. 6.

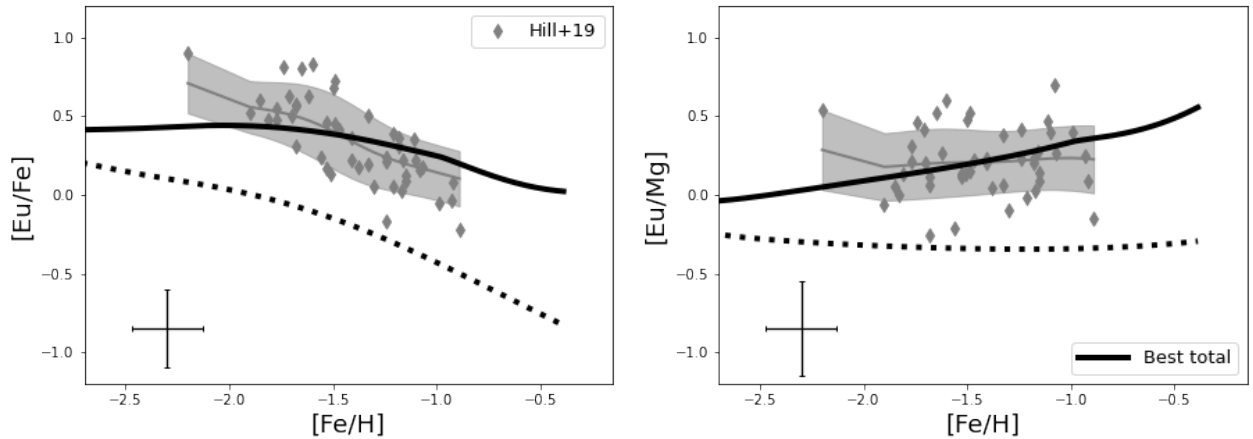


Fig. 11. [Eu/Fe] vs [Fe/H] (left panel) and [Eu/Mg] versus [Fe/H] (right panel) for Sculptor for models with increased MNS production at low metallicity. Solid lines represent evolutionary tracks for the model adopting the Eu enrichment setup with maximum total weighted likelihood for Sagittarius and Fornax. For comparison, the model with standard Eu enrichment setup is also shown (dotted lines). The legend is the same as in Fig. 6.

chemical evolution studies (e.g. Siegel et al. 2019; Prantzos et al. 2020).

For their prompt nature, such events closely follow the SFR in galaxies: for this reason we do not need to repeat the analysis performed for MNSs and consider the ‘missing Eu’ production rate and metallicity threshold found in Section 5. The ‘missing

Eu’ rate shown in Fig. 8 translates in an increase in the Eu production by prompt events of a factor of ≈ 4.4 . Considering the results for individual galaxies, we find a range between ≈ 3.1 (for Scl dSph) and ≈ 6.1 (for For dSph).

The boosted Eu production could be due either to an augmented event rate or to an increased Eu yield. In particular, if

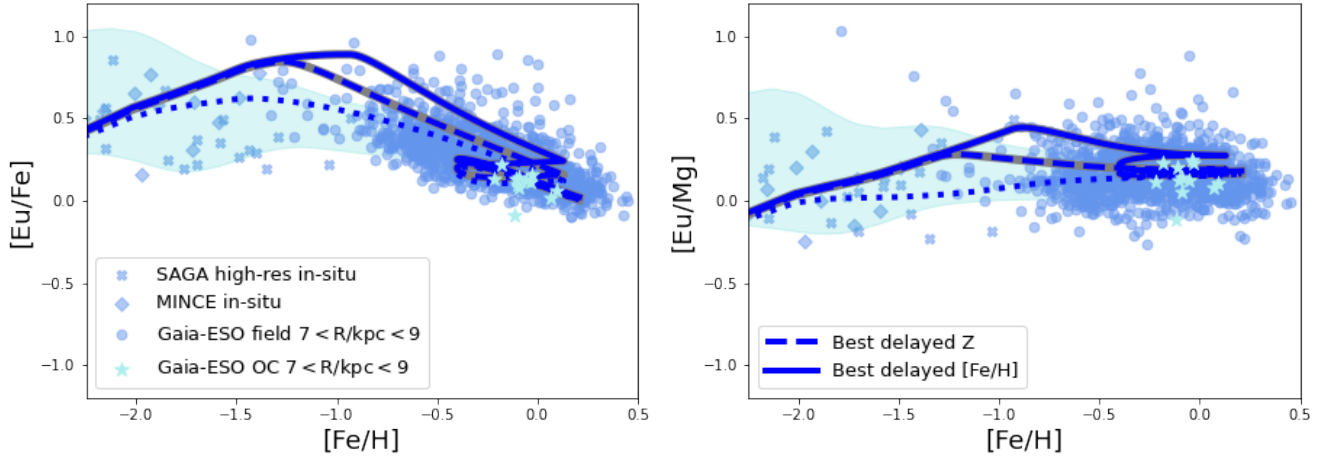


Fig. 12. [Eu/Fe] vs [Fe/H] (left panel) and [Eu/Mg] versus [Fe/H] (right panel) for the MW for models with increased MNS production at low metallicity. Solid lines represent evolutionary tracks for models with Eu enrichment setup as the best model for Local Group dwarfs, while dashed lines models for which the MW galaxy has a metallicity threshold Z corresponding to the $[\text{Fe}/\text{H}]_{\text{thresh}}$ as computed for Local Group dwarfs. For comparison, the model with standard Eu enrichment setup is also shown (dotted lines). Data legend is as in Fig. 5.

we assume a fixed $\alpha_{\text{MRD}} = 0.2$ (see Table 1), an increase in the Eu production by a factor of 4.4 implies an (average) Eu yield by MRD-SNe of $\approx 2 \times 10^{-6} M_{\odot}$. Similar values are obtained in MRD-SNe simulations assuming larger magnetic field strength (e.g. model L0.6 of Nishimura et al. 2017); therefore, leaving the door open for larger yield values. On the other hand, if we assume a total r-process production per collapsar $> 0.1 M_{\odot}$ (Siegel et al. 2019), resulting in an Eu yield of $\geq 10^{-5} M_{\odot}$ (assuming a solar scaled r-process pattern, Arnould et al. 2007), this would imply that $\lesssim 5\%$ of very massive stars ($m > 20 M_{\odot}$) are progenitors of collapsar events. Again, such values are theoretically possible according to the ratio of SN Ib/c and long GRB rate¹ ($\lesssim 1\%$, Ghirlanda & Salvaterra 2022 and references therein) and the observed fraction of SNe Ib/c which correspond to very massive stars and not stripped binaries ($\approx 10\%$, Karamahmetoglu et al. 2023).

It is clear that all the solutions to the problem of Eu underproduction in LG dwarf galaxies invoking an increased contribution to Eu enrichment from prompt sources are highly degenerate. The safest fix at our stage rests, perhaps, on the possibility of an increased prompt event rate so as to match the observations in LG dwarfs.

6.3. Applying the new scenarios to the MW

In the subsections above, we advocate for a boost in Eu production from either prompt or delayed stellar sources below a given metallicity threshold to match the theoretical predictions of our chemical evolution models for LG dSphs to the observations. In the remainder of this section, we will see whether our new Eu enrichment scenario can be applied to the MW, without leading to inconsistencies with the data.

The [Eu/Fe] and [Eu/Mg] versus [Fe/H] abundance patterns for the MW model with an increased Eu production by MNS systems formed at low metallicity (with parameters from the best model for dwarf galaxies, i.e. $\alpha_{\text{incr}} = 40$, $[\text{Fe}/\text{H}]_{\text{thresh}} = -0.95$ dex) are shown with the solid lines in Fig. 12. As expected,

¹ The collapsar model (MacFadyen & Woosley 1999; Woosley & Heger 2006) is one of the favourite scenarios for long GRB events, originating from the explosion of a single, very massive ($m \gg 10 M_{\odot}$) rotating star that collapses to form a rapidly rotating black hole.

for both [Eu/Fe] and [Eu/Mg] the model shows a peak approximately at $[\text{Fe}/\text{H}] \approx -0.9/-0.8$ dex $\geq [\text{Fe}/\text{H}]_{\text{thresh}}$. However, the peak [Eu/X] ratios are well above the confidence interval of the data trend. This is especially the case for [Eu/Fe] (Fig. 12 left panel), where the model predictions are up to $\sim 0.3-0.4$ dex above the upper end of the confidence interval of the observed trend.

However, by looking at the $[\text{Fe}/\text{H}]_{\text{thresh}}$ values obtained from the maximum likelihood analysis on the individual Sgr and For dSphs (see Fig. 9, red and green points), $[\text{Fe}/\text{H}] = -1$ dex and $[\text{Fe}/\text{H}] = -0.9$ dex, respectively, we note that they correspond to similar global metallicities, namely $Z \approx 2.2 \times 10^{-3}$ for Sgr and $Z \approx 1.8 \times 10^{-3}$ for For. In turn, these translate into solar-scaled metallicities between ≈ 0.105 and $0.13 Z_{\odot}$ (assuming Z_{\odot} from Grevesse & Sauval 1998) or ≈ 0.13 and $0.16 Z_{\odot}$ (assuming Z_{\odot} from Asplund et al. 2009).

On this regard, it is worth saying that the differences between the SFHs of dSphs and more star forming systems lead to different chemical enrichment patterns. This is due to the time-delay model (e.g. Matteucci 2012, 2021), for which the evolution of [X/Fe] versus [Fe/H] patterns are different depending on the galaxy star formation. As α -elements, such as oxygen, show enhanced/depleted $[\alpha/\text{Fe}]$ at a given [Fe/H] in systems with larger/lower star formation rate and being oxygen the metal dominating the global metallicity Z budget, variations in the galaxy star formation rate influence the relation between [Fe/H] and Z . Therefore, the MW galaxy should exhibit the Z metallicities corresponding to the $[\text{Fe}/\text{H}]_{\text{thresh}}$ of dwarf systems at lower [Fe/H]. Indeed, we find that for our MW model, $[\text{Fe}/\text{H}] \approx -1.33$ dex at $Z \approx 2 \times 10^{-3}$. Therefore, we run an additional model for the MW where we assume the same α_{incr} factor as found from the best model in Section 6, but assuming a lower $[\text{Fe}/\text{H}]_{\text{thresh}}$, namely -1.33 dex, corresponding to a $Z \approx 2 \times 10^{-3}$ in the MW. The results for this additional model are displayed with dashed lines in Fig. 12. Now, the model predictions align much better with the observed trends, lying within the 1σ confidence interval in [Eu/Mg] and just slightly above it ($\lesssim 0.1$ dex) in [Eu/Fe]. In this context, it is also important to emphasize that when discussing metallicity, we should carefully distinguish between using global Z and the stellar [Fe/H].

The important uncertainties in the modelling of r-process (yields, nucleosynthetic sources fraction within the IMF; see e.g. Molero et al. 2021 and references therein) even for our

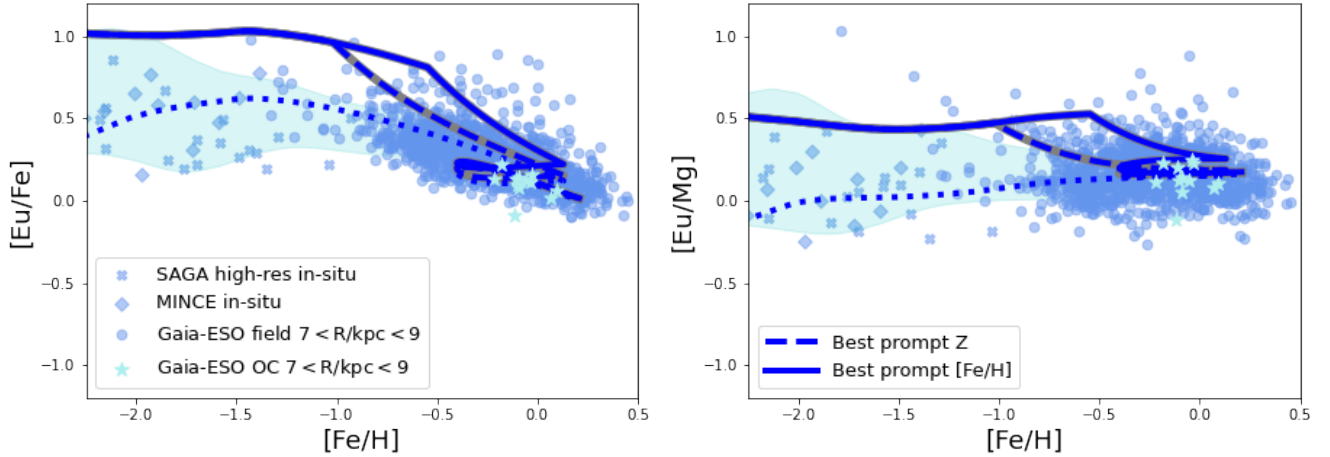


Fig. 13. [Eu/Fe] vs [Fe/H] (left panel) and [Eu/Mg] vs [Fe/H] (right panel) for the MW models with increased prompt sources (MRD-SNe and/or collapsars) production at low metallicity. Solid lines represent evolutionary tracks for models with Eu enrichment setup as the best model for Local Group dwarfs, while dashed lines models for which the MW galaxy has a metallicity threshold Z corresponding to the $[\text{Fe}/\text{H}]_{\text{thresh}}$ as computed for Local Group dwarfs. For comparison, the model with standard Eu enrichment setup is also shown (dotted lines). Data legend is as in Figs. 5 and 12.

Galaxy imply that such marginal disagreement in the trends can be recovered with few minor adjustments in some of the free r -process parameters (e.g. α_{MRD} , MRD yields) without compromising the reproduction of observables (e.g. the present-day MNS rate). Moreover, the small discrepancy shown by this model may be also explained by uncertainties in the derivation of Eu stellar abundances, with $\langle 3D \rangle$ and NLTE corrections that increase the median [Eu/Fe] trend in the MW of around ~ 0.1 dex at $[\text{Fe}/\text{H}] \sim -1.5$ – -1 dex (see e.g. Fig. 8 by Guo et al. 2025). The same line of reasoning cannot be applied to the model shown with the solid lines in Fig. 12, because of the much more severe offset (up to ~ 0.3 – 0.4 dex) with the observations.

We repeated the kind of analysis outlined above in the case of a putative increased production of Eu from prompt sources (MRD-SNe and/or collapsars) at low metallicity. In particular, the solid lines in Fig. 13 refer to a MW model with parameters from the best-fitting model for dwarf galaxies (‘missing Eu’ rate = $5 \cdot 10^{-10}$, $[\text{Fe}/\text{H}]_{\text{thresh}} = -0.55$ dex; see Section 5). In addition, we show the results of a model with increased prompt sources production, but with a lower $[\text{Fe}/\text{H}]_{\text{thresh}}$, corresponding to the global metallicity Z as found for the [Fe/H] threshold in Sgr and For. In particular, we apply a $[\text{Fe}/\text{H}]_{\text{thresh}} \approx -1.02$ dex, corresponding in our MW model to $Z = 3.5 \cdot 10^{-3} \approx 0.21 Z_{\odot}$ (assuming Z_{\odot} from Grevesse & Sauval 1998); namely, in between the values found for Sgr ($Z \approx 4.7 \cdot 10^{-3}$) and For ($Z \approx 2.7 \cdot 10^{-3}$) individually.

Looking at the model with metallicity threshold calibrated on [Fe/H] it is clear that the boost of Eu production from prompt sources leads to a general overestimation of the observed Eu content in the Galaxy even beyond the adopted threshold of $[\text{Fe}/\text{H}] = -0.55$ dex. For [Eu/Fe], in particular (see Fig. 13, left panel), the model predicts a low-metallicity plateau with extreme values ($[\text{Eu}/\text{Fe}] \approx 1$ dex), which disagrees with the average trend spotted in the data. The situation is slightly better in the [Eu/Mg] vs [Fe/H] plane (Fig. 13, right panel), where the trend predicted by the model remains within the 1σ confidence interval of the data up to $[\text{Fe}/\text{H}] \approx -1.5$ dex. However, also in this case the high plateau ($[\text{Eu}/\text{Mg}] \approx 0.5$ dex) prevents the agreement with the bulk of the data at larger metallicities, confirming the overproduction of Eu in the MW by this model.

When we apply the threshold on the global metallicity, Z , rather than on [Fe/H], the agreement between model predictions

and data does not improve substantially. In fact, despite the shorter plateau predicted for [Eu/Fe] and [Eu/Mg], the model tracks still severely overestimate the observed trend up to $[\text{Fe}/\text{H}] \gtrsim -1$ dex. Therefore, the results displayed in Fig. 13 indicate the inability of the scenario favouring Eu production from prompt events to explain the abundance patterns in the MW, excluding it as a possible way to reconcile the trends in the MW and LG dwarf galaxies.

7. Discussion and conclusions

In this study, we investigated the chemical enrichment of the r -process element Europium in galaxies of the Local Group by means of detailed models of chemical evolution, considering both a prompt (among the hypotheses, magneto-rotationally driven supernovae; hereafter, MRD-SNe, e.g. Winteler et al. 2012, or collapsars, e.g. Siegel et al. 2019) and a delayed (merging of compact objects and/or neutron stars; hereafter, MNSs, e.g. Argast et al. 2004) source of enrichment.

In particular, we focused on the simultaneous modelling of Eu abundance patterns observed in the Milky Way and in the three most massive dwarf Spheroidal galaxies of the LG, namely Sagittarius, Fornax, and Sculptor. This effort is necessary, as Eu has started to be used as a possible chemical tag for accreted structures in the field of Galactic Archaeology (see e.g. Monty et al. 2024) but we are currently lacking a detailed theoretical understanding of the evolution of this element in different galactic systems. In fact, apart from the very metal-poor regime ($[\text{Fe}/\text{H}] \lesssim -2$ dex), most theoretical works only focused on Eu evolution in the MW galaxy. To answer to this need, we started from a well-tested model that reproduces all the available observables in the MW disk (Molero et al. 2023) and expand the same setup for Eu enrichment (nucleosynthesis sources, yields and delay in the pollution for MNSs) to models tailored to reproduce the star formation histories, the lighter elements abundance ratios (e.g. $[\alpha/\text{Fe}]$) and the metallicity distribution functions of Sgr, For and Scl.

Following this approach, the main conclusions of this work can be summarised as follows:

- the ‘standard’ set-up adopted for Eu enrichment, which reproduces both the measured abundance trends and the event rates in the MW well (see Molero et al. 2023 and

Figs. 4 and 5), significantly underestimates the [Eu/Fe] abundance ratio in the three most massive LG dSphs (Sgr, For, Scl). In particular, the model predictions underestimate the observed [Eu/Fe] trend by ~ 0.5 dex for all three galaxies (see Fig. 6);

- we quantify the amount of ‘missing Eu’ and its extent in metallicity in LG dwarf galaxies. To reproduce the observed trends in LG dSphs, we need an additional Eu production rate (normalised to the SFR) of $\approx 5 \cdot 10^{-10}$ up to metallicities $[\text{Fe}/\text{H}] \approx -0.5/-0.6$ dex, with similar results for the different galaxies (see Fig. 7). By comparing the result with the production rates from MNSs and MRD-SNe, we find that a boost of a factor of ≈ 4 in the Eu production rate is needed to reconcile the model predictions with the observations;
- searching for the origin of this ‘missing Eu’, we explored two possible scenarios: (i) a larger contribution by MNS systems (or delayed scenario) or (ii) an increment in the production by MRD-SNe or collapsars (prompt scenario), both at low-metallicity.

For the delayed scenario, we find that we need to increase the produced Eu from MNSs by a factor of ≈ 40 from the systems forming at $[\text{Fe}/\text{H}] \lesssim -1$ dex (see Fig. 9). For the prompt scenario, the increase in Eu production we propose (≈ 4.5) is compatible with theoretical values found by both the MRD-SNe (e.g. Nishimura et al. 2017) and collapsars models (Siegel et al. 2019; Ghirlanda & Salvaterra 2022; Karamahmetoglu et al. 2023) and needs to extend up to $[\text{Fe}/\text{H}] \lesssim -0.6$ dex;

- both the delayed and the prompt scenarios that explain the LG dwarf galaxy data are applied to the chemical evolution model for the MW, to check whether or not these scenarios are compatible with the chemical trends found in the Solar Neighbourhood. The resulting [Eu/Fe] and [Eu/Mg] versus [Fe/H] abundance patterns (see solid lines in Figs. 12 and 13) are generally above the observed trends, with the MW model adopting the prompt scenario overestimating the observed trend up to ~ 0.4 dex and the delayed scenario by ~ 0.3 dex;
- nonetheless, if we consider the global metallicity Z instead of [Fe/H] as a threshold for the delayed scenario (see dashed lines in Fig. 12)², the model predictions are in fairly good agreement with the observations, with discrepancies ($\lesssim 0.1$ dex). It may be ascribable to limitations in the modelling of r-process elements chemical enrichment (e.g. Côté et al. 2019; Molero et al. 2021, 2023) or derivation of Eu abundances from spectral lines (e.g. Mashonkina et al. 2017; Guo et al. 2025).

In turn, this suggests the delayed scenario as a possible solution to theoretically reconcile the trends observed in the MW and in LG dwarfs without advocating intrinsic differences in the stellar populations of the galaxies. Moreover, the present analysis emphasize that in discussing metallicity, we should carefully distinguish between using global Z and the stellar [Fe/H] when discussing the properties of stellar populations, such as MNS progenitor systems.

Summarizing, our results proved that an increased production of Eu by MNS systems forming at low metallicity ($Z \lesssim 0.1 Z_{\odot}$) may be seen as a viable scenario to explain the Eu enrichment of different galaxies in the LG. However, due to the severe degeneracies still affecting the models, we cannot reach a conclusive assessment of Eu evolution in LG galaxies. On the one hand,

despite the statistically meaningful approach adopted here, the limited sizes of the samples of stars with Eu abundance determinations in LG dwarfs prevent us to capture small variations in the parameters characterizing the proposed enrichment scenarios. On the other hand, modelling the chemical evolution of r-process elements in general presents multiple challenges, with extremely limited knowledge and ambiguities persisting even in the most basic ingredients for chemical evolution models. As an example, stellar yields from candidate Eu polluters are extremely poorly sampled in terms of progenitors masses and metallicity, so that chemical evolution models still have to rely on single point grids (see also Molero et al. 2025 for a discussion on this point).

Nonetheless, this work highlights the importance of considering galactic ecosystems different from the MW in the modelling of neutron-capture element evolution and in particular Eu, which is the main tracer of r-process production. In fact, by looking at galaxies with different SFHs, we can mitigate the degeneracies in the r-process modelling and shed light on the nature of the different nucleosynthetic sources.

Further targeting of neutron-capture elements in LG galaxies (also including, e.g. the more massive and interacting Magellanic Clouds) is certainly needed to fill the gaps in our understanding, building samples that are statistically significant and complete over the metallicity range spanned by LG galaxies. In this regards, upcoming facilities such as 4MOST (de Jong et al. 2012) will reserve a significant amount of time on the galaxies object of this study, allowing us to increase the number of observed stars with abundances of neutron-capture elements by several orders of magnitude (Skúladóttir et al. 2023).

Acknowledgements. The authors thank the referee for the careful reading of the manuscript and the comments provided. MP thanks F. Matteucci for the insightful discussions and suggestions on the paper content. MP, DR, and AM acknowledge financial support from the project “LEGO – Reconstructing the building blocks of the Galaxy by chemical tagging” granted by the Italian MUR through contract PRIN2022LLP8TK_001. MM thanks the support from the Deutsche Forschungsgemeinschaft (DFG, German Research Foundation) – Project-ID 279384907 – SFB 1245, the State of Hessen within the Research Cluster ELEMENTS (Project ID 500/10.006).

References

- Abbott, B. P., Abbott, R., Abbott, T. D., et al. 2017, *Phys. Rev. Lett.*, **119**, 161101
- Abbott, R., Abbott, T. D., Abraham, S., et al. 2021, *ApJ*, **913**, L7
- Alencastro Puls, A., Kuske, J., Hansen, C. J., et al. 2025, *A&A*, **693**, A294
- Alexander, R. K., Vincenzo, F., Ji, A. P., et al. 2023, *MNRAS*, **522**, 5415
- Arcones, A., & Thielemann, F.-K. 2023, *A&A Rev.*, **31**, 1
- Argast, D., Samland, M., Thielemann, F. K., & Qian, Y. Z. 2004, *A&A*, **416**, 997
- Arnould, M., Goriely, S., & Takahashi, K. 2007, *Phys. Rep.*, **450**, 97
- Asplund, M., Grevesse, N., Sauval, A. J., & Scott, P. 2009, *ARA&A*, **47**, 481
- Bettinelli, M., Hidalgo, S. L., Cassisi, S., et al. 2019, *MNRAS*, **487**, 5862
- Bisterzo, S., Gallino, R., Straniero, O., Cristallo, S., & Käppeler, F. 2011, *MNRAS*, **418**, 284
- Bogomazov, A. I., Lipunov, V. M., & Tutukov, A. V. 2007, *Astron. Rep.*, **51**, 308
- Burris, D. L., Pilachowski, C. A., Armandroff, T. E., et al. 2000, *ApJ*, **544**, 302
- Cappellaro, E., Turatto, M., Tsvetkov, D. Y., et al. 1997, *A&A*, **322**, 431
- Cavallo, L., Cescutti, G., & Matteucci, F. 2021, *MNRAS*, **503**, 1
- Cavallo, L., Cescutti, G., & Matteucci, F. 2023, *A&A*, **674**, A130
- Cescutti, G., Romano, D., Matteucci, F., Chiappini, C., & Hirschi, R. 2015, *A&A*, **577**, A139
- Cescutti, G., Bonifacio, P., Caffau, E., et al. 2022, *A&A*, **668**, A168
- Chiappini, C., Matteucci, F., & Gratton, R. 1997, *ApJ*, **477**, 765
- Chiappini, C., Matteucci, F., & Romano, D. 2001, *ApJ*, **554**, 1044
- Côté, B., Belczynski, K., Fryer, C. L., et al. 2017, *ApJ*, **836**, 230
- Côté, B., Eichler, M., Arcones, A., et al. 2019, *ApJ*, **875**, 106
- Cowan, J. J., Sneden, C., Lawler, J. E., et al. 2021, *Rev. Mod. Phys.*, **93**, 015002
- de Boer, T. J. L., Tolstoy, E., Hill, V., et al. 2012, *A&A*, **544**, A73
- de Boer, T. J. L., Belokurov, V., & Koposov, S. 2015, *MNRAS*, **451**, 3489
- de Jong, R. S., Bellido-Tirado, O., Chiappini, C., et al. 2012, *SPIE Conf. Ser.*, **8446**, 84460T

² In practice, we consider a [Fe/H] threshold for which the MW galaxy has a metallicity Z corresponding to the [Fe/H] threshold as computed for LG dwarfs.

- Dolphin, A. E. 2002, *MNRAS*, 332, 91
- Fernandes, H., Feuillet, D., Feltzing, S., & Skúladóttir, Á. 2024, *A&A*, 691, A333
- Fernandes, L., Mason, A. C., Horta, D., et al. 2023, *MNRAS*, 519, 3611
- François, P., Cescutti, G., Bonifacio, P., et al. 2024, *A&A*, 686, A295
- Ghirlanda, G., & Salvaterra, R. 2022, *ApJ*, 932, 10
- Giacobbo, N., & Mapelli, M. 2018, *MNRAS*, 480, 2011
- Gilmore, G., Randich, S., Worley, C. C., et al. 2022, *A&A*, 666, A120
- Greggio, L., Simonetti, P., & Matteucci, F. 2021, *MNRAS*, 500, 1755
- Grevesse, N., & Sauval, A. J. 1998, *Space Sci. Rev.*, 85, 161
- Grichener, A., & Soker, N. 2019, *ApJ*, 878, 24
- Grichener, A., Kobayashi, C., & Soker, N. 2022, *ApJ*, 926, L9
- Grisoni, V., Cescutti, G., Matteucci, F., et al. 2020, *MNRAS*, 492, 2828
- Guo, Y., Storm, N., Bergemann, M., et al. 2025, *A&A*, 693, A211
- Hansen, C. J., Primas, F., Hartman, H., et al. 2012, *A&A*, 545, A31
- Hansen, C. J., Montes, F., & Arcones, A. 2014, *ApJ*, 797, 123
- Hansen, C. J., El-Souri, M., Monaco, L., et al. 2018, *ApJ*, 855, 83
- Hartwig, T., Ishigaki, M. N., Klessen, R. S., & Yoshida, N. 2019, *MNRAS*, 482, 1204
- Hill, V., Skúladóttir, Á., Tolstoy, E., et al. 2019, *A&A*, 626, A15
- Hirai, Y., Ishimaru, Y., Saitoh, T. R., et al. 2015, *ApJ*, 814, 41
- Hopkins, P. F., Gurvich, A. B., Shen, X., et al. 2023, *MNRAS*, 525, 2241
- Horta, D., Schiavon, R. P., Mackereth, J. T., et al. 2021, *MNRAS*, 500, 1385
- Hotokozaka, K., Beniamini, P., & Piran, T. 2018, *Int. J. Mod. Phys. D*, 27, 1842005
- Ishigaki, M. N., Aoki, W., & Chiba, M. 2013, *ApJ*, 771, 67
- Iwamoto, K., Brachwitz, F., Nomoto, K., et al. 1999, *ApJS*, 125, 439
- Jeřábková, T., Hasani Zonoozi, A., Kroupa, P., et al. 2018, *A&A*, 620, A39
- Ji, A. P., Frebel, A., Chiti, A., & Simon, J. D. 2016a, *Nature*, 531, 610
- Ji, A. P., Frebel, A., Simon, J. D., & Chiti, A. 2016b, *ApJ*, 830, 93
- Kalogera, V., Kim, C., Lorimer, D. R., et al. 2004, *ApJ*, 601, L179
- Karakas, A. I. 2010, *MNRAS*, 403, 1413
- Karamehmetoglu, E., Sollerman, J., Taddia, F., et al. 2023, *A&A*, 678, A87
- Kennicutt, Robert C., J. 1998, *ApJ*, 498, 541
- Kobayashi, C., Leung, S.-C., & Nomoto, K. 2020, *ApJ*, 895, 138
- Korobkin, O., Rosswog, S., Arcones, A., & Winteler, C. 2012, *MNRAS*, 426, 1940
- Kroupa, P., Tout, C. A., & Gilmore, G. 1993, *MNRAS*, 262, 545
- Lanfranchi, G. A., & Matteucci, F. 2004, *MNRAS*, 351, 1338
- Lanfranchi, G. A., Matteucci, F., & Cescutti, G. 2008, *A&A*, 481, 635
- Law, D. R., & Majewski, S. R. 2016, in *Astrophysics and Space Science Library*, 420, Tidal Streams in the Local Group and Beyond, eds. H. J. Newberg, & J. L. Carlin, 31
- Lemasle, B., de Boer, T. J. L., Hill, V., et al. 2014, *A&A*, 572, A88
- Letarte, B., Hill, V., Tolstoy, E., et al. 2010, *A&A*, 523, A17
- Letarte, B., Hill, V., Tolstoy, E., et al. 2018, *A&A*, 613, C1
- Li, H., Aoki, W., Matsuno, T., et al. 2022, *ApJ*, 931, 147
- Liberatori, A., Alvarez Garay, D. A., Palla, M., et al. 2025, *A&A*, in press, <https://doi.org/10.1051/0004-6361/202554412>
- Lombardo, L., Hansen, C. J., Rizzuti, F., et al. 2025, *A&A*, 693, A293
- MacFadyen, A. I., & Woosley, S. E. 1999, *ApJ*, 524, 262
- Magrini, L., Viscasillas Vázquez, C., Spina, L., et al. 2023, *A&A*, 669, A119
- Marcon-Uchida, M. M., Matteucci, F., & Costa, R. D. D. 2010, *A&A*, 520, A35
- Mashonkina, L., Jablonka, P., Pakhomov, Y., Sitnova, T., & North, P. 2017, *A&A*, 604, A129
- Matsuno, T., Hirai, Y., Tarumi, Y., et al. 2021, *A&A*, 650, A110
- Matteucci, F. 2012, *Chemical Evolution of Galaxies* (Springer-Verlag Berlin Heidelberg)
- Matteucci, F. 2021, *A&A Rev.*, 29, 5
- Matteucci, F., & Brocato, E. 1990, *ApJ*, 365, 539
- Matteucci, F., & Recchi, S. 2001, *ApJ*, 558, 351
- Matteucci, F., Spitoni, E., Recchi, S., & Valiante, R. 2009, *A&A*, 501, 531
- Matteucci, F., Romano, D., Arcones, A., Korobkin, O., & Rosswog, S. 2014, *MNRAS*, 438, 2177
- McKenzie, M., Yong, D., Marino, A. F., et al. 2022, *MNRAS*, 516, 3515
- McMillan, P. J. 2017, *MNRAS*, 465, 76
- McWilliam, A., Wallerstein, G., & Mottini, M. 2013, *ApJ*, 778, 149
- Melioli, C., Brighenti, F., D'Ercole, A., & de Gouveia Dal Pino, E. M. 2009, *MNRAS*, 399, 1089
- Mennekens, N., & Vanbeveren, D. 2014, *A&A*, 564, A134
- Minelli, A., Bellazzini, M., Mucciarelli, A., et al. 2023, *A&A*, 669, A54
- Mishenina, T. V., & Kovtyukh, V. V. 2001, *A&A*, 370, 951
- Molero, M., Romano, D., Reichert, M., et al. 2021, *MNRAS*, 505, 2913
- Molero, M., Magrini, L., Matteucci, F., et al. 2023, *MNRAS*, 523, 2974
- Molero, M., Magrini, L., Palla, M., et al. 2025, *A&A*, 694, A274
- Monaco, L., Bellazzini, M., Bonifacio, P., et al. 2007, *A&A*, 464, 201
- Monty, S., Belokurov, V., Sanders, J. L., et al. 2024, *MNRAS*, 533, 2420
- Mucciarelli, A., Bellazzini, M., Ibata, R., et al. 2017, *A&A*, 605, A46
- Nishimura, N., Takiwaki, T., & Thielemann, F.-K. 2015, *ApJ*, 810, 109
- Nishimura, N., Sawai, H., Takiwaki, T., Yamada, S., & Thielemann, F. K. 2017, *ApJ*, 836, L21
- Nomoto, K., Kobayashi, C., & Tominaga, N. 2013, *ARA&A*, 51, 457
- Palla, M. 2021, *MNRAS*, 503, 3216
- Palla, M., Matteucci, F., Calura, F., & Longo, F. 2020a, *ApJ*, 889, 4
- Palla, M., Matteucci, F., Spitoni, E., Vincenzo, F., & Grisoni, V. 2020b, *MNRAS*, 498, 1710
- Palla, M., Santos-Peral, P., Recio-Blanco, A., & Matteucci, F. 2022, *A&A*, 663, A125
- Palla, M., De Looze, I., Relaño, M., et al. 2024a, *MNRAS*, 528, 2407
- Palla, M., Magrini, L., Spitoni, E., et al. 2024b, *A&A*, 690, A334
- Patel, A., Metzger, B. D., Cehula, J., et al. 2025, *ApJ*, 984, L29
- Prantzos, N., Abia, C., Cristallo, S., Limongi, M., & Chieffi, A. 2020, *MNRAS*, 491, 1832
- Randich, S., Gilmore, G., Magrini, L., et al. 2022, *A&A*, 666, A121
- Reichert, M., Hansen, C. J., Hanke, M., et al. 2020, *A&A*, 641, A127
- Reichert, M., Obergaulinger, M., Eichler, M., Aloy, M. Á., & Arcones, A. 2021, *MNRAS*, 501, 5733
- Reichert, M., Obergaulinger, M., Aloy, M. Á., et al. 2023, *MNRAS*, 518, 1557
- Roederer, I. U. 2011, *ApJ*, 732, L17
- Roederer, I. U., Preston, G. W., Thompson, I. B., et al. 2014, *AJ*, 147, 136
- Romano, D., Karakas, A. I., Tosi, M., & Matteucci, F. 2010, *A&A*, 522, A32
- Romano, D., Bellazzini, M., Starkenburg, E., & Leaman, R. 2015, *MNRAS*, 446, 4220
- Romano, D., Magrini, L., Randich, S., et al. 2021, *A&A*, 653, A72
- Rozwadowska, K., Vissani, F., & Cappellaro, E. 2021, *New A*, 83, 101498
- Schönrich, R. A., & Weinberg, D. H. 2019, *MNRAS*, 487, 580
- Siegel, M. H., Dotter, A., Majewski, S. R., et al. 2007, *ApJ*, 667, L57
- Siegel, D. M., Barnes, J., & Metzger, B. D. 2019, *Nature*, 569, 241
- Simon, J. D., Brown, T. M., Mutlu-Pakdil, B., et al. 2023, *ApJ*, 944, 43
- Simonetti, P., Matteucci, F., Greggio, L., & Cescutti, G. 2019, *MNRAS*, 486, 2896
- Skúladóttir, Á., & Salvadori, S. 2020, *A&A*, 634, L2
- Skúladóttir, Á., Puls, A. A., Amarsi, A. M., et al. 2023, *The Messenger*, 190, 19
- Spina, L., Magrini, L., & Cunha, K. 2022, *Universe*, 8, 87
- Spitoni, E., Matteucci, F., Recchi, S., Cescutti, G., & Pipino, A. 2009, *A&A*, 504, 87
- Spitoni, E., Silva Aguirre, V., Matteucci, F., Calura, F., & Grisoni, V. 2019, *A&A*, 623, A60
- Spitoni, E., Verma, K., Silva Aguirre, V., & Calura, F. 2020, *A&A*, 635, A58
- Spitoni, E., Verma, K., Silva Aguirre, V., et al. 2021, *A&A*, 647, A73
- Suda, T., Katsuta, Y., Yamada, S., et al. 2008, *PASJ*, 60, 1159
- Thielemann, F. K., Eichler, M., Panov, I. V., & Wehmeyer, B. 2017, *Annu. Rev. Nucl. Part. Sci.*, 67, 253
- Tsujimoto, T. 2021, *ApJ*, 920, L32
- Van der Swaelmen, M., Viscasillas Vázquez, C., Cescutti, G., et al. 2023, *A&A*, 670, A129
- Vasini, A., Spitoni, E., & Matteucci, F. 2024, *A&A*, 683, A121
- Vincenzo, F., Matteucci, F., Vattakunnel, S., & Lanfranchi, G. A. 2014, *MNRAS*, 441, 1815
- Vincenzo, F., Matteucci, F., Recchi, S., et al. 2015, *MNRAS*, 449, 1327
- Viscasillas Vázquez, C., Magrini, L., Casali, G., et al. 2022, *A&A*, 660, A135
- Wanajo, S., Hirai, Y., & Prantzos, N. 2021, *MNRAS*, 505, 5862
- Watson, D., Hansen, C. J., Selsing, J., et al. 2019, *Nature*, 574, 497
- Winteler, C., Käppeli, R., Perego, A., et al. 2012, *ApJ*, 750, L22
- Woosley, S. E., & Heger, A. 2006, *ApJ*, 637, 914

Appendix A: Maximum likelihood calculations

In the main text, we show the results of the likelihood computation performed on the grid of parameters $\Theta = \{\text{'Missing Eu' rate, [Fe/H]_{\text{thresh}}}\}$ (in the 'missing Eu' case; Section 5) and $\Theta = \{\alpha_{\text{incr}}, [\text{Fe/H}]_{\text{thresh}}\}$ (in the MNS increased production case; Section 6.1). In doing this, we adopt a similar procedure to what illustrated in Spitoni et al. (2020, 2021). In the following, we show the details on how we perform these computations.

For each individual galaxy, the set of observables is $x_{\text{gal}} = \{[\text{Fe}/\text{H}], [\text{Eu}/\text{Fe}], \text{ and } [\text{Eu}/\text{Mg}]\}$, while the set of model parameters is $\Theta = \{\text{var}_1, \text{var}_2\}$ (where var_1 and var_2 are as in the cases illustrated above). The likelihood, \mathcal{L} , assuming that the uncertainties on the observables are normally distributed, can be therefore written as:

$$\ln \mathcal{L}_{\text{gal}} = - \sum_{n=1}^{N_{\text{gal}}} \ln \left((2\pi)^{d/2} \prod_{j=1}^d \sigma_{n,j} \right) - \frac{1}{2} \sum_{n=1}^{N_{\text{gal}}} \sum_{j=1}^d \left(\frac{x_{n,j} - \mu_{n,j}}{\sigma_{n,j}} \right)^2, \quad (\text{A.1})$$

where N is the number of stars for the individual galaxy. The quantities $x_{n,j}$ and $\sigma_{n,j}$ are respectively the measured value of j -th observable and its uncertainty for n -th star in the individual galaxy, whereas $\mu_{n,j}$ is the model value for to the j -th observable associated to the n -th star.

To associate to each star the corresponding predicted value by the chemical evolution model we compute the closest value on the curve given a data point $x_{n,j}$ as in Spitoni et al. (2020), namely defining the following 'data-model distance' function D :

$$D_{n,j} = \sqrt{\sum_{i=1}^d \left(\frac{x_{n,j} - \mu_{n,ji}}{\sigma_{n,j}} \right)^2}, \quad (\text{A.2})$$

where i runs over a set of discrete values on the curve. Hence, the closest point on the curve will be $\mu_{n,j} = \mu_{n,ji_0}$, which fulfils the following condition:

$$S_n \equiv \min_i \{D_{n,j}\} = \sqrt{\sum_{j=1}^d \left(\frac{x_{n,j} - \mu_{n,ji_0}}{\sigma_{n,j}} \right)^2}. \quad (\text{A.3})$$

After the computation of the likelihood for the individual galaxies, we then calculate a 'total weighted' likelihood over the set of galaxies. To do that, we weight the log likelihood for each individual galaxy according to the number stars observed within it, as shown in the following equation:

$$\text{Weighted}(\ln \mathcal{L}_{\text{tot}}) = \sum_{\text{gal}} \ln \mathcal{L}_{\text{gal}} \times N_{\text{gal}}. \quad (\text{A.4})$$

In this way, we avoid to underweight or overweight the likelihood for the individual galaxies accordingly to the different sizes of the samples (e.g. ~ 40 stars for Sgr, ~ 110 for For).

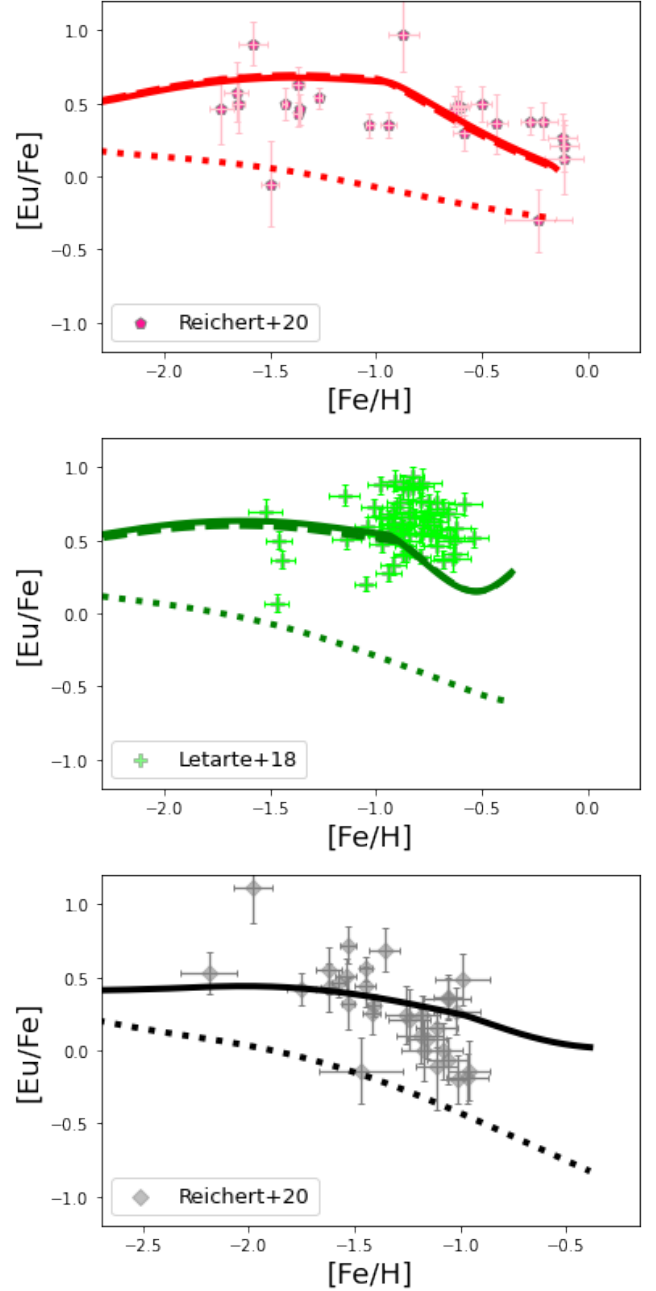


Fig. B.1. $[\text{Eu}/\text{Fe}]$ vs $[\text{Fe}/\text{H}]$ for Sagittarius (top panel), Fornax (central panel) and Sculptor (bottom panel) for models with increased MNS production at low metallicity and different datasets to the ones described in Section 2.2. Data are from Reichert et al. 2020 (Sagittarius and Sculptor) and Letarte et al. (2010, 2018) (Fornax). The legend is the same as in Figs. 10 and 11.

Appendix B: Testing on additional datasets for local dwarf galaxies

As we mention in Section 6, we compare the best models emerged from our likelihood analysis (see Appendix A) to other available datasets for the LG dwarf galaxies analysed in this work.

In particular, here we consider the datasets from Reichert et al. (2020) for Sgr and Scl and the one by Letarte et al. (2010, 2018) for For dSph. These additional datasets are not considered

in our main analysis as due to the disadvantages they present relative to the adopted samples. These are, for example, the smaller samples with available Eu abundances (Sgr, For, Scl), the less careful stellar selection (Sgr), the lower spectral resolution in the observations (Sgr, Scl). Moreover, the non-negligible overlap in the catalogues of For and Scl (~ 70 and ~ 35 stars, respectively) does not allow to increase significantly the number of stars observed in each galaxy, and therefore their addition would not be beneficial for the study.

The resulting best models with increased Eu production from MNSs (see Section 6.1), together with the ones adopting the standard scenario for Eu enrichment, are compared with these other datasets in Fig. B.1.

This figure confirms the findings in the main text, with the standard scenario unable to fulfil the Eu production needed in the different LG dwarfs. Indeed, models with an additional r-process production component at low metallicity (in this case, from MNSs) are necessary to fill the gap with [Eu/Fe] observations.